Energy 278 (2023) 127954

Contents lists available at ScienceDirect

Energy

journal homepage: www.elsevier.com/locate/energy

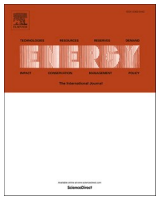

Extremes and resource assessment of wind and waves in central Mediterranean Sea

Valentina Laface, Felice Arena *

Mediterranea University of Reggio Calabria, Natural Ocean Engineering Laboratory (NOEL), Italy

ARTICLE INFO

Handling Editor: G Iglesias

Keywords:
Wind energy
Wave energy
Renewable energy
Storm
Wind speed
Wave height

ABSTRACT

This paper deals with extremes and resource assessment of wind and waves in central Mediterranean Sea. The extreme value analysis is performed following Equivalent Storm Models (ESMs) approach, commonly employed in the context of significant wave height return values estimation. In this work, it is extended to wind storm events thanks to some analogies between wave and wind processes at short and long-term scale. The Equivalent Exponential Storm (EES) Model is selected for this study because of its realistic description of actual events time evolution. Energy estimations are based on both real storm data and EES model. The input data used for this analysis comes from the re-analysis of atmospheric and wave conditions performed by MeteOcean group at DICCA of Genoa University and cover the period from January 1979 to December 2020. Sixteen points have been selected including the south and west coast of the Italian peninsula, the Sicily and Sardinia Islands. The study is focused on return values estimation and energy assessment, mainly related on the storm concept; it aims to elucidate analogies and/or differences of wind and wave at a given site as well as how the two resources are distributed along the examined locations, identifying the potential working time over the year and which are the storm events providing the prevalent energetic contribution to harvestable energy. Results show that the location characterized by the severest wind storm and wave storm events do not coincide and not always the location where the severest storm occur is also the most energetic site. Further, the variability of return values with different levels of return period for wind speeds is lower than for significant wave heights: this aspect is motivated by a shape parameter of Weibull distribution that is systematically higher for the wind speed with respect to the significant wave height. The extremes of significant wave height are more variable from one location to another than those of wind speed ones and the same behavior is exhibited by energy resources, elucidating that the wind resource in the investigated sites is more homogeneous.

1. Introduction

In the last decades, the increase of energy demand and the need of reduction of energy consumption from fossil fuels have conducted to a fast development of the renewables energy sector. This factor has led the research community to focus their investigations on renewable energy relates aspects, from themes connected with resource assessment and climate analysis, to those concerning the patenting and developing of prominent devices for energy harvesting. Wind and wave resources have received a great interest because although their intermittence over time they are characterized by a considerable energy content. In a worldwide context, Mediterranean area has a significant delay in the implementation of marine renewable energy projects with respect to other maritime areas, like Atlantic Ocean, Pacific Ocean and North Sea. Exploitation of Marine Renewable Energy (MRE) potential in the Mediterranean is crucial to contribute to the global and European efforts towards decarbonization, in the framework of the UN Sustainable Development Goals (SDG7 Affordable and Clean Energy and SDG13 Climate Action) as well as the European Green Deal. There are several studies evaluating the feasibility and performances of wind [1–3] and wave [4–6] plants in the Mediterranean Sea. In this context, the selection of areas to be destinated to renewable energy farms plays a key role in the success of the project. In this regard, an optimized resource assessment is paramount, but not sufficient to support all the decisions involved in the site selection. In fact, any energy device has to both convert the incoming resource and has to face with the environmental loads. For this reason, a good practice is to combine resource assessment studies with extreme value estimations for a complete climate characterization. To this the necessity to

* Corresponding author.
E-mail addresses: valentina.laface@unirc.it (V. Laface), arena@unirc.it (F. Arena).

https://doi.org/10.1016/j.energy.2023.127954
Received 4 January 2023; Received in revised form 14 April 2023; Accepted 26 May 2023
Available online 27 May 2023

have reliable data with a large space and temporal coverage, arises. This problem is overcome thanks to meteorological models that simulate weather and sea conditions using validated atmospheric and wave numerical models with the generation of large hindcast databases [7–12]. In the literature a great body of works investigated wave power [12–15], wind power [16–18] and both [19–22] in various locations in Mediterranean area. Numerous are the studies on extreme values of wind speed and wave height [23–27] and investigating the Mediterranean climate in general [27,28]. There is a lack of studies dealing with combined wind and wave resource assessment and wind and wave extreme value analysis in central Mediterranean Sea. Thus, this paper is focused on wind and waves extremes and resource assessments mainly based on storm concept in central Mediterranean Sea. The scope of this work is to provide an exhaustive overview of the wind and wave energy and extremes variability over the investigated area useful for site selection for offshore wind and wave farms. It also, aspires to represent a kind of atlas to be used as input for preliminary design of wind and wave energy harvesters at the examined locations. In this regard, it is very important to couple energy assessment, statistics in general and extreme values analysis, when evaluating the feasibility and potentiality of a wind and/or wave farms project. Statistics influence the operability and energy yield of the device and extreme events are paramount for adequate design of the structural part. Sites characterized by the greatest amount of both wind and wave available energy are identified. Further, a storm analysis is performed to detect the storm events responsible of the most relevant contribution to total available and useable energy and those involving downtime periods as well, comparing wind and wave cases. The paper is organized as follows: section 2 describes methods used for this analysis, section 3 provides an on overview on the input data, section 3 is dedicated to data analysis and results and section 4 gives the conclusions.

2. The Equivalent Exponential Storm model

The Equivalent Exponential Storm (EES) Model [29] belongs to the class of Storm Models [29–33] that represents a relatively new approach introduced in the context of long-term analysis of sea storms. It is based on the substitution of actual storm sequence at a given site (actual sea) with a simplified storm sequence whose peculiarity is that all the storms have the same shape and are fully characterized by an intensity and a duration parameter, established in relation to actual storm event. Specifically, the storm intensity is fixed equal to the peak of the actual storm and the duration parameter is determined by imposing an equality between a relevant statistic parameter of actual and associated simplified storm (e. g. the maximum expected wave height for the wave case). In this regard, depending on the objective of the analysis, one have the possibility to set the duration parameter in order to establish an equivalence between actual and simplified storm that is more related to the investigated aspect. For example, if the analysis is only targeted to estimation of energy content of the storm the duration can be fixed such that the total energy of the storm is the same in actual and simplified event. When more aspect are involved in the analysis, as in the case of this work, one can select a unique equivalence and use the same storm duration for all the analyses. The simplified storm can be triangular [30], power [31], exponential [29] or trapezoidal [32] in shape, but the logic behind the model remains the same. In fact, whatever the shape is, due to its simple mathematical description it is possible to develop analytical solutions for the calculation of return period of storms with assigned characteristics. The main aspect justifying the use of such analytical solutions is related with the statistical equivalence between actual and associated simplified storm. Jointly, it is assumed that the exceedance probability of either significant wave height or wind speed for high thresholds coincide in actual and simplified storm sequence. The two conditions mentioned above ensure that the actual storm sequence and the simplified one are characterized by the same risk. Thus, the return period derived on the basis of simplified storm sequence is the same of that estimated from a real storm sequence. Another strength of this approach with respect to classical ones, is that it provides a temporal evolution of events once their intensity and duration parameters are known. In this regard, there is also some recent some recent literature on statistical models for “storm trajectories” which can be used in place of “equivalent storm” profiles [34–36]. The knowledge of process evolution over time allows the possibility to develop formulas that could be very useful for energy related studies e. g. storm energy content. Further, identified an operation range of either wind speed or significant wave height at a given site, it is possible to estimate operation time and amount of useable energy of each storm event. Focusing on the EES, the simplified storm is defined by an exponential law depending on intensity and duration parameters and on the threshold used for actual storm identification.

2.1. The wave storm model

The EES model has been developed in the context of the calculation of return value of significant wave height. It provides a closed analytical solution for the calculation of the return period $R(H_s > h)$ of a storm during which the maximum significant wave height exceeds the threshold h. It has been derived on the basis of general definition of return period, as the ratio between a long time interval τ and the number $N(h;\tau)$ of storms occurring during τ whose maximum significant wave height exceeds h:

$$R(H_s > h) = \frac{\tau}{N(h;\tau)} \tag{1}$$

The number $N(h;\tau)$ depends on the probability density function of EES peaks $p_A(a)$ as follows [29,30,32]:

$$N(h;\tau) = N(\tau)\int_h^{\infty} p_A(a)da \tag{2}$$

where $N(\tau)$ is the total number of storms occurring during τ and $p_A(a)$ is the probability density function of storm peaks a.

The EES probability density function $p_A(a)$ has been derived analytically by imposing that the total time during which the significant wave height is above the threshold h is the same in actual storm and EES sequence [29] (see Appendix A1 for key points on analytical derivation of $p_A(a)$). The time above the threshold h in a EES with assigned intensity a and duration b is calculated starting from the temporal evolution of significant wave height $H_s(t)$, that for an EES is expressed as [29]:

$$h(t) = a\exp\left[\frac{2}{b}\ln\left(\frac{h_{crit}}{a}\right)|t|\right] \tag{3}$$

where h_{crit} is the threshold used for actual storm identification (usually 1.5 times the average significant wave height at site), a and b are the EES

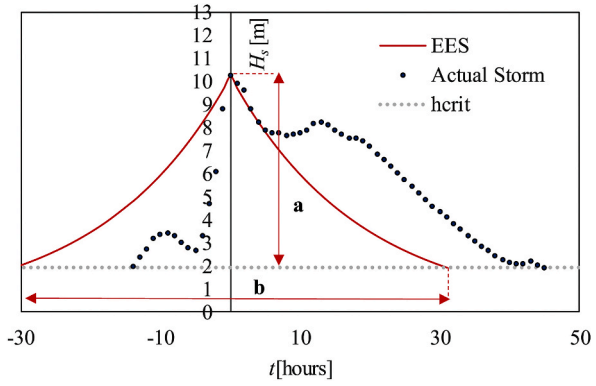

Fig. 1. Example of actual wave storm and associated EES.

intensity and duration (see Fig. 1), respectively. The parameter a is fixed equal to the maximum significant wave height of actual storm, while duration parameter b is determined by an iterative procedure.

With the above assumptions, $p_A(a)$ is explicated as

$$p_A(a) = -\frac{\tau}{N(\tau)}\frac{1}{b_m(a)}\ln\left(\frac{h_{crit}}{a}\right)\left[\frac{dP(H_s>a)}{da}+a\frac{d^2P(H_s>a)}{da^2}\right] \tag{4}$$

and the analytical form of the return period $R(H_s > h)$ became:

$$R(Hs>h) = \frac{b_m(h)}{-h\ln\left(\frac{h_{crit}}{h}\right)p(H_s=h)+P(H_s>h)} \tag{5a}$$

where $p(H_s = h) = -dP(H_s > h)/dh$ is the probability density function of H_s, $P(H_s > h)$ the exceedance probability and $b_m(a)$ is a regression function relating the average value of storm duration to the storm intensity. It depends on the specific site because is calculated using the EESs a and b parameters of each storm. Note that equation (5a) is valid for any distribution assumed for significant wave height. Further, this specific analytical form is related with the exponential shape (3) used to describe the EES temporal evolution. A different storm shape leads to a different analytical form, but still depending on intensity-duration regression function and probability distribution of significant wave height. Considering a two parameter Weibull distribution for the significant wave height, equation (5a) becames:

$$R(Hs>h) = \frac{b_m(h)}{\left[1-h\ln\left(\frac{h_{crit}}{h}\right)\left(\frac{u}{w}\right)\left(\frac{h}{w}\right)^{(u-1)}\right]}\exp\left[\left(\frac{h}{w}\right)^u\right] \tag{5b}$$

where u and w are the shape and scale parameters of the Weibull distribution. In this regard, note that the probability distribution $P(H_s > h)$ is determined by processing the whole data sample of H_s without any consideration on EES concept, because it is assumed that the $P(H_s > h)$ of actual sea and EESs sequence are the same.

Now, focusing on the regression function b_m(a) it is worth to say that its determination represents the most demanding step in applying the EES model. It requires a previous identification of all the actual storm event from data with the subsequent calculation of intensity a and duration b for each of the associated EES. The intensity parameter a is assumed equal to the maximum significant wave height during actual storm (see Fig. 1), while duration parameter b is calculated by following an iterative procedure imposing the equality between the maximum expected wave heights of actual and exponential storm. The maximum expected wave height of a sea storm can be calculated following the Borgman approach [37,38] while the expression of EES maximum expected wave height can be derived from the Borgman one, that is useable for any storm shape, by explicating it for an EES shape, taking into account the relation (3) between significant wave height and time. The following form is achieved [29]:

$$\overline{H}_{\max}(a,b,h_{crit}) = \int_0^{\infty}1-\exp\left\{-\frac{b}{\ln\left(\frac{h_{crit}}{a}\right)}\int_{h_{crit}}^{a}\frac{1}{\overline{T}(h)}\ln[1-P(H;H_s=h)]\frac{1}{h}dh\right\}dH \tag{6}$$

where $P(H; H_s = h)$ is the distribution of crest to trough individual wave height, while $\overline{T}(h)$ is the mean zero up-crossing wave period in a sea state with significant wave height equal to h.

The above expression is function of the duration parameter b. Starting from a tentatively value of b, the maximum expected wave height of EES is calculated and compared with the Borgmann estimation for actual storm, if it is smaller, one has to increment b otherwise to reduce and proceed until the equality is satisfied with a reasonable margin of error. It has been numerically proven that the above equality not only leads to the equivalence of the areas under the exceedance probability curves of the maximum wave height of AS and EES, but on the superposition of the two at any individual wave height threshold as well, providing a full statistic equivalence between AS and EES. Once the couples of parameters (a, b) of EESs are known, storms are divided within classes of storm intensity 1 m wide and for each class the average intensity a_m and duration b_m are calculated. Then, data are fitted by an exponential law like the following:

$$b_m(a) = k_1\exp(k_2 a) \tag{7}$$

where k_1 and k_2 are in hours and m^{-1}, respectively.

As mentioned above, the fact that the EES model provides a law describing the time evolution of H_s, makes possible to calculate the storm energy and other interesting quantities in the context of wave energy harvesting. In this regard, starting from the power associated to a given sea state in deep water [13]:

$$P_{s\ wave}(H_s,T_m,\gamma_f) = \frac{\rho g^2}{64\pi}\gamma_f H_s^2 T_m \tag{8}$$

where ρ is the sea water density, g is the acceleration due to gravity, γ_f is a parameter depending on the spectrum that is equal to 1.12 for a mean Jonswap and 1.15 for Pierson Moskowtiz, H_s is the sea state significant wave height and T_m is the mean wave period.

A formula of the storm energy is simply achieved by integrating (8) over the storm duration as:

$$E_{\ actual\ storm} = \int_0^D P_{s\ wave}(t)dt \tag{9}$$

Then, considering that the mean wave period T_m can be related directly to the significant wave height, as [39]:

$$T_m = K_m(\alpha_{PH},\gamma)\sqrt{\frac{H_s}{g}} \tag{10}$$

being K_m a constant depending on the spectral shape through the Philips parameter α_{PH} and the peak enhancement factor γ of the Jonswap spectrum, equation (8) can be further simplified as:

$$P_{s\ wave}(H_s) = C_{wave}H_s^{2.5} \tag{11}$$

where C_{wave} is a constant including the effects of water density, acceleration due to gravity and spectral shape.

As demonstrated by Ref. [13], introducing a JONSWAP-like approximation on the frequency spectrum allows reliable estimation of the wave power even in case of bimodal seas. In this regard, if a mean JONSWAP spectrum is considered, $C_{wave} = \rho g^{1.5}c$ and c ≈ 0.0578.

Then, using relation (9), rewriting it for an EES and changing from variable t to h:

$$\begin{aligned}E_{TOT\ EES_{wave}}(a,b,h_{crit}) &= 2C_{wave}\int_0^{b/2}h^{2.5}(t)dt = -2C_{wave}\frac{b}{2}\frac{1}{\ln\left(\frac{h_{crit}}{a}\right)}\int_{h_{crit}}^{a}h^{2.5}\frac{1}{h}dh\\ &= C_{wave}\frac{-b}{\ln\left(\frac{h_{crit}}{a}\right)}\frac{1}{2.5}\left(a^{2.5}-h_{crit}^{2.5}\right)\end{aligned} \tag{12}$$

Considering that the operation range for a given device is defined by a lower and upper limits of working thresholds, $h_{cut\ in}$, $h_{cut\ out}$, the useable storm energy and related operation time are given by:

$$E_{usable\ EES\ wave}(a,b,h_{crit}) = \begin{cases} 0 \quad if \ \ a \le h_{cut\ in} \\ E_{TOT\ EES\ wave} \ if \ \ h_{cut\ in} \ < \ a \le h_{cut\ out} \\ C_{wave}[-b/\ln(h_{crit}/a)](1/2.5)\left(h_{cut\ out}^{2.5} - h_{cut\ in}^{2.5}\right) \quad if \ a > h_{cut\ out} \end{cases} \tag{13}$$

$$t_{operation\ \ EES\ wave}(a,b,h_{crit}) = \begin{cases} 0 \quad if \quad a \le h_{cut\ in} \\ b \quad if \quad h_{cut\ in} < a \le h_{cut\ out} \\ b[1 - \ln(h_{cut\ out}/a)/\ln(h_{crit}/a)] \quad if \ a > \ h_{cut\ out} \end{cases} \tag{14}$$

Note that $h_{cut\ in}$ represents the minimum value of H_s necessary to justify the activation of the device, while $h_{cut\ out}$ is the maximum value of H_s within which the device can operate in safety condition. For $h_{cut\ in}$ a value of 1–1.5 m is reasonable and is always smaller or equal than the critical threshold h_{crit} in Mediterranean Sea. This means that during storm events with peak smaller or equal than $h_{cut\ out}$ the device can be always operative.

2.2. The wind storm model

The idea behind the utilization of EES model for long-term analysis of wind speeds arises from some consideration highlighting significant analogies between wave and wind processes at both short-term and long-term scales [40]. A sea storm is a non-stationary process during which the significant wave height varies over time: grows, reaches a peak and decreases in relation with an established critical threshold h_{crit}. This phenomenon is schematized as a sequence of stationary processes named sea states, during which the sea surface elevation is a gaussian process characterized by a given frequency spectrum. Similarly, in the case of wind process at long-term scale we talk about a wind storm whose evolution is analogous to that of H_s of a wave storm and is defined by a sequence of wind states during which the average wind speed V_m exceeds a critical threshold v_{crit}. At short-term scale wind is described by wind speed fluctuations around an average wind speed V_m, called turbulence. Wind turbulence is a zero mean process characterized by a turbulence intensity TI and frequency spectrum. The TI is defined as the ratio between standard deviation of wind speed fluctuations and average wind speed. Both wind and waves at short-term scale are modelled as gaussian processes. Focusing on long-term scale, due to the analogous time evolution of wave storm and wind storm, the shapes introduced for wave storm analysis are suitable for wind storm as well. Thus, the wind speed of an exponential wind storm over time evolves as:

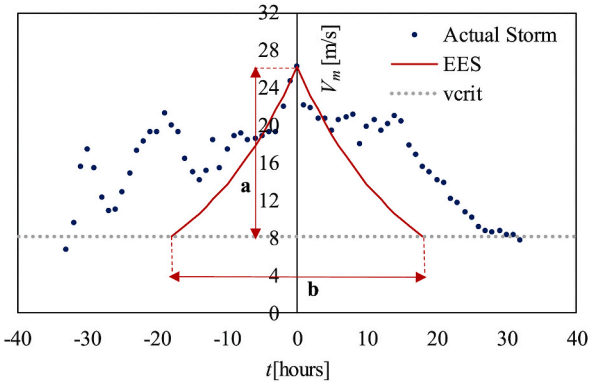

Fig. 2. Example of actual wind storm and associated EES.

$$V_m(t) = a \exp\left[\frac{2}{b}\ln\left(\frac{v_{crit}}{a}\right)|t|\right] \tag{15}$$

where v_{crit} is the threshold used for actual wind storm identification, a is the EES intensity equal to the maximum average wind speed during actual wind storm and b is the EES duration (see Fig. 2).

Further, considering that the analytical development of the return period (5a) is based only on the storm shape described by equation (3), even changing the variable that evolves over time and thus using equation (15), the general solution (5a) is also valid for wind process if H_s is replaced with V_m. Further, considering that average wind speeds follow a Weibull distribution as well, the return period $R(V_m > v)$ of a wind storm during which the maximum average wind speed exceeds the threshold v is given by:

$$R(V_m > v) = \frac{b_m(v)}{\left[1 - u_{wind}\ \ln\left(\frac{v_{crit}}{v}\right)\left(\frac{u_{wind}}{w_{wind}}\right)\left(\frac{v}{w_{wind}}\right)^{(u_{wind}-1)}\right]} \exp\left[\left(\frac{v}{w_{wind}}\right)^{u_{wind}}\right] \tag{16}$$

Note, that the function at the numerator is the regression function relating the average storm duration to the average storm intensity. Even for wind storm a regression of the form (7) is an adequate option, with the difference that in this case k_2 is in measured s/m and a (or equivalently v) is in m/s. The last aspect to be clarified in the adaptation of EES model to the wind storm case is related with the EES duration calculation. In fact, for the wave storm it was calculated iteratively by imposing the equality between the maximum expected wave heights of actual storm and EES.

In this regard, a way to establish a procedure for the calculation of EES duration by constraining the equality between a relevant statistical actual storm and EES wind parameter is needed. A suitable candidate could be the maximum expected gust speed. A wind gust consists in a change of wind speed over a given small time interval and can be arbitrarily defined as any discrete events that can be identified from turbulent flow [41], that is any discrete velocity-time events that can be extrapolated from a turbulence time series. Accordingly, in the context of this paper, wind gust is defined as the amplitude G of wind turbulence process. Assuming that wind turbulence is a Gaussian process, the gust G defined above has a Rayleigh distribution $P(G;\sigma)$ of the form:

$$P(G;\sigma) = \exp\left[-\frac{1}{2}\left(\frac{G}{\sigma}\right)^2\right] \tag{17}$$

where σ is the standard deviation of wind turbulence.

Further, applying the Borgman approach adopted for wave height, to wind gust G as defined above, the maximum expected gust for an actual wind storm can be expressed as [42]:

$$\overline{G}_{\max\ AS} = \int_0^\infty 1 - \exp\left\{\int_0^D \frac{1}{\overline{T}(u(t))}\ln[1 - P(G;\sigma)]dt\right\}dG \tag{18}$$

where $\overline{T}(u)$ is the mean zero up crossing period of wind turbulence associated to an average wind speed u and turbulence intensity $TI{=}\sigma/u$, as described in the following. For the calculation of $\overline{T}(u)$ see Appendix A2.

Then, with same logic of wave storm case, the solution (18) is adapted to an exponential shape and the maximum expected wind gust of an EES is obtained:

$$\overline{G}_{\max\ EES}(a,b,v_{crit}) = \int_0^{\infty} 1 - \exp\left\{ -\frac{b}{\ln\left(\frac{v_{crit}}{a}\right)} \int_{v_{crit}}^{a} \frac{1}{\overline{\overline{T}}(v)} \ln[1 - P(G;\sigma)] \frac{1}{v} dv \right\} dG \tag{19}$$

Finally, focusing on the energetic aspects, the specific wind power $P_{s\ wind}$ associated with a wind state with assigned average wind speed V_m is given by:

$$P_{s\ wind}(V_m) = \frac{1}{2}\rho_{air} V_m^3 \tag{20}$$

where ρ_{air} is the air density.

In analogy to what has been done for the wave storm case described in previous subsection, the total energy associated with a wind EES is given by:

$$E_{TOT\ EES wind}(a,b,v_{crit}) = 2\frac{1}{2}\rho_{air}\int_0^{b/2} v^3(t)dt = -\rho_{air}\frac{b}{2\ln\left(\frac{v_{crit}}{a}\right)}\int_{v_{crit}}^{a} v^3\frac{1}{v}dv = -\frac{1}{6}\rho_{air}\frac{b}{\ln\left(\frac{v_{crit}}{a}\right)}\left(a^3 - v_{crit}^3\right) \tag{21}$$

Then considering the operational range of an offshore wind turbine, defined by a cut in wind speed $v_{cut\ in}$ and a cut out wind speed $v_{cut\ out}$ the useable energy and operation time of an assigned EES are given by:

$$E_{usable\ EES win}(a,b,v_{crit}) = \begin{cases} 0 \quad if \quad a \le v_{cut\ in} \\ E_{TOT\ EES\ wind} \quad if \quad v_{cut\ in} < a \le v_{cut\ out} \\ -(1/6)\rho_{air}[b/\ln(v_{crit}/a)]\left(v_{cut\ out}^3 - v_{crit}^3\right) \quad if\ a > v_{cut\ out} \end{cases} \tag{22}$$

$$t_{operation\ \ EES\ wind}(a,b,v_{crit}) = \begin{cases} 0 \quad if \quad a \le v_{cut\ in} \\ b \quad if \quad h_{cut\ in} < a \le v_{cut\ out} \\ b[1 - \ln(v_{cut\ out}/a)/\ln(v_{crit}/a)] \quad if\ a > v_{cut\ out} \end{cases} \tag{23}$$

Note that offshore wind turbines have an operational range that is between wind speed of 5 m/s and 25 m/s. A cut in wind speed of 5 m/s is always smaller than the critical threshold v_{crit} used for wind storm identification. Thus, for storms with peak lower or equal to cut out wind speed $v_{cut\ out}$ the wind turbine is always operative and all storm energy can be utilized.

3. Input data

The input data used for this work are those provided by DICCA MeteOcean Re-Analysis database (http://www3.dicca.unige.it/meteocean/hindcast.html). This database is obtained by a re-analysis of atmospheric and wave condition and covers the period from January 1979 to the end of December 2018 for all the Mediterranean Sea. Meteorological re-analyses have been developed employing NCEP Climate Forecast System Reanalysis, CFSR for the period from January 1979 to December 2010 and CFSv2 for the period January 2011 to December 2018. The numerical model chain employed for the construction of this database consists in a meteorological model for the reanalysis and simulation of winds and atmospheric fields and a third generation model for the description of generation and propagation of wind and swell waves in the Mediterranean basin. The wind forcing employed in the simulations has been provided by the 10-m wind fields obtained using the non-hydrostatic mesoscale model WRF-ARW version 3.3.1 [43]. A single computational domain has been implemented for the WRF model, covering the whole Mediterranean with a ~10 km resolution Lambert conformal grid. Initial and boundary conditions for the atmospheric simulations with the WRF model were provided from the CFSR (Climate Forecast System Reanalysis) database [44]. The re-analysis of wave conditions relies on the third generation wave model WavewatchIII (WWIII), version 3.14 [45,46], for the description of wave generation and evolution processes of the wave field. Following the set-up employed for wind simulations, WWIII has been implemented in the Mediterranean basin on a regular grid (hereinafter referred to as R10) with a resolution of 0.1273 × 0.09°, corresponding almost to 10 km at the latitude of 45°N, and ETOPO1 data has been used for the interpolation on the computational grid of the bathymetry. The model has been forced with the wind fields obtained from the atmospheric model with an hourly time step. Validation of the hindcast has been developed through the comparison between the numerical results and wave buoy observations [47,48]. Data are provided every hour and several parameters are given. Among them are: Hs - Significant Wave Height [m], Tm - Mean Period [s], Tp - Peak Period [s], Dirm - Mean Direction [°N], Dirp - Peak Direction [°N] and Wind Velocity [m/s]. For the scope of this work only significant wave height and wind speed data are considered.

4. Data analysis

This section proposes a data analysis aiming to provide an exhaustive assessment of extreme values and power characteristics of wind and waves in central Mediterranean Sea. For this purpose, a set of sixteen points has been selected from the DICCA database, covering the West and South coasts of Italian peninsula, Sardinia and Sicily islands (see Fig. 3 and Table 1 for geographic coordinates and water depths). Data analysis is carried out by processing average wind speed and significant wave height time series. The first part of the work is dedicated on return values calculation via EES model in order to identify which are the locations where the severest wind and wave storms occur and how extremes vary from one location to another. Then, follows an estimation of annual available energy, average power and a storm energy based analysis finalized to the identification of storm events providing the most energetic contribution to available energy, their average number of occurrences during the year, amount of useable energy and related operation time for all the storms.

4.1. Extreme value analysis of wind speed and significant wave height

This subsection shows the results of extreme value analysis for both significant wave height and wind speed. The analysis is assessed on the basis of EES model described in previous section. Essentially, the use of such model for the calculation of return values of either significant wave height or wind speeds requires the determination of the probability distribution, the actual storm identification, the calculation of associated EES parameters and determination of the regression function. Both significant wave height and wind speed are well represented by a two parameter Weibull distribution, that is the selected one for this work. For what concerns actual storm identification accordingly to Ref. [40] a threshold of 1.5 times the averages of wind speeds and significant wave heights are assumed. In this context, a sea storm is considered as a sequence of sea states during which the significant wave height exceeds the threshold $h_{crit} = 1.5\overline{H}_s$ and analogously a wind storm as a sequence of wind states during which average wind speed exceeds the threshold $v_{crit} = 1.5\overline{V}_m$. Actual storm events identification has been performed according to the above definitions. Then, the parameters of associated EES have been calculated following the procedure explained in previous

Fig. 3. Location of the investigated sites.

Table 1
Geographic coordinate and water depth of the selected points.

Point	Name	Lat[°N]	Long[°E]	Depth[m]
000292	1	44.13	8.998	1420.8
001468	2	42.51	10.6534	276.28
002415	3	41.61	12.054	618.6
004524	4	40.08	14.728	407.4
005827	5	39.36	15.6194	627.27
007259	6	38.64	15.492	927.37
009041	7	37.74	15.6194	1787.01
009046	8	37.74	16.256	1841.76
007446	9	38.55	17.02	1345.21
006355	10	39.09	17.6567	1495.16
009609	11	37.47	15.492	2069.46
010598	12	37.02	13.3274	553.99
007787	13	38.37	13.3274	960.42
004049	14	40.35	7.9793	287.1
005776	15	39.36	7.9793	322.15
004644	16	39.99	10.144	1336.69

Table 2
Shape and scale parameters of the wind and wave Weibull distributions.

Point	u_{wave}	W_{wave}[m]	u_{wind}	W_{wind}[m/s]
1	1.153	0.824	1.673	5.766
2	1.051	0.655	1.834	6.475
3	1.083	0.826	1.858	6.446
4	1.048	0.829	1.702	5.987
5	1.006	0.794	1.575	5.734
6	0.982	0.694	1.601	5.794
7	1.062	0.671	1.768	5.930
8	1.097	0.848	1.685	5.823
9	1.133	0.897	1.969	6.959
10	1.234	1.059	1.851	7.003
11	1.107	0.751	1.884	6.011
12	1.182	1.028	1.917	6.987
13	1.099	0.920	1.646	6.140
14	1.241	1.371	1.834	6.728
15	1.238	1.384	1.865	6.940
16	1.019	0.770	1.691	5.732

section and finally the two regression functions have been determined. Table 2 summarizes the shape and scales parameters of significant wave height and average wind speed Weibull distribution.

Return values at different level of return period R are represented in Fig. 4 in the top and bottom panels for significant wave height and wind speed, respectively, and are listed in Table 3. From a first analysis, it is evident that the significant wave height return values exhibit a high variability among the selected sites. In particular, for a return period $R = 1$ year the maximum variability of return values among the considered locations is about 48%, it reduces for increasing return period and is about 43% for $R = 100$ years. The less severe storms occur at points 1, 2, 7, 11 that are all located in different areas. Further, as expecting the severest storms occur off the west coast of Sardinia. Focusing on a single location, the variability of return values of significant wave height associated with R between 1 year and 100 years ranges from a minimum of about 39% at point 10 to maximum of 48% at points 5 and 6. This last aspect is strongly related to the values assumed by the shape parameter $u_{\text{wave.}}$ that regulates the ratio of return values at different probability levels. Accordingly, it is seen that the highest values of the parameters u_{wave} is that of the location showing the smallest variability of return values with R, while the smallest u_{wave} corresponds to the location characterized by the highest return values variability. Now, focusing on results related to average wind speed analysis, it can be seen that the return values show a significantly lower variability among the considered location at any return period R, in comparison to the wave case. Such variability is minimum for $R = 1$year and is about 15% and maximum for $R = 100$ years at which is about 19%. This result may reveal a more homogeneous distribution of wind resource along the examined locations. Focusing on a single point is evident that the variability of wind speed return values with return period R is smaller in comparison with significant wave height case and varies from a minimum of about 23% at point 9 to a maximum of 29% at point 5. This aspect is easily motivated by comparing the values of shape parameter of significant wave height and wind speed distributions at each point. In fact, shape parameter regulates the ratios of return values at different probability levels and the wind shape parameter is always greater than

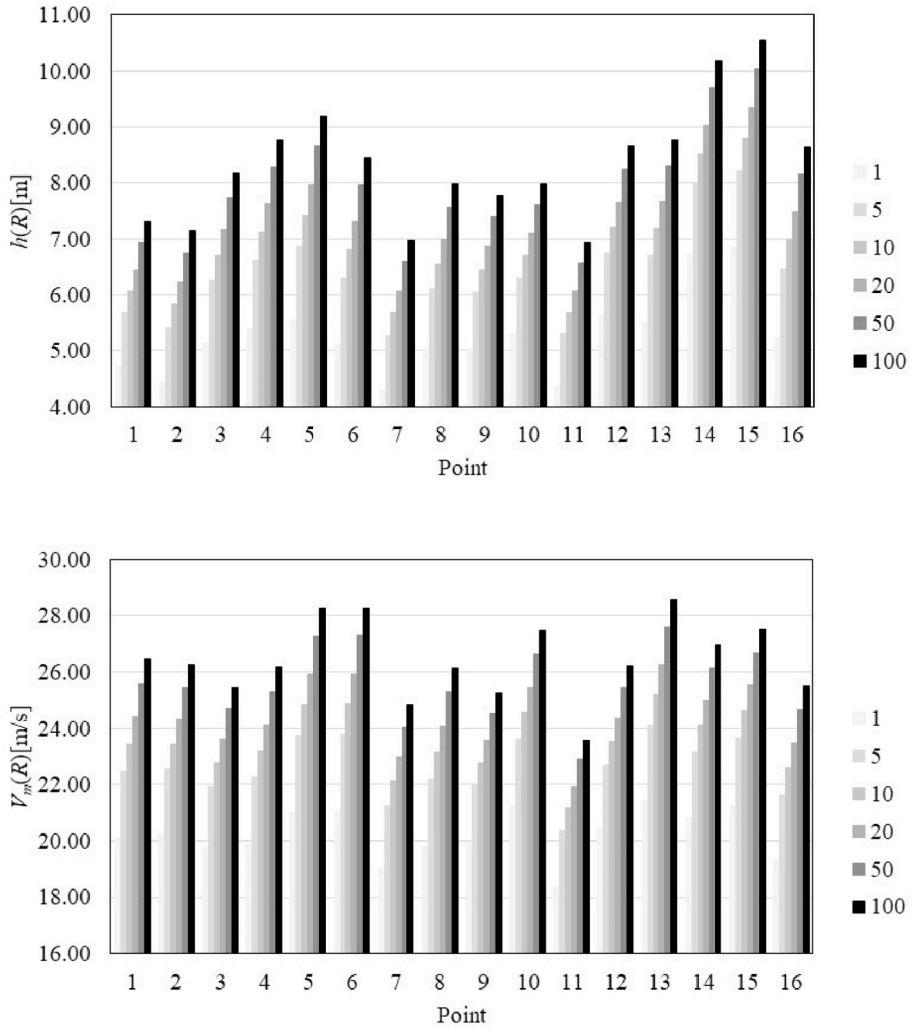

Fig. 4. Return values of significant wave height H_s (R) (top) and average wind speed V_m (R) (bottom) for return periods R = 1, 5, 10, 20, 50, 100 years.

Table 3
Return values of significant wave height H_s (R) and average wind speed V_m (R) for return periods R = 1, 5, 10, 20, 50, 100 years.

Point	$H_s(R)$						$V_m(R)$					
1	4.7	5.7	6.1	6.4	6.9	7.3	20.1	22.5	23.5	24.4	25.6	26.5
2	4.4	5.4	5.8	6.2	6.7	7.1	20.2	22.5	23.5	24.3	25.4	26.2
3	5.1	6.2	6.7	7.2	7.7	8.2	19.7	21.9	22.8	23.6	24.7	25.4
4	5.4	6.6	7.1	7.6	8.3	8.8	19.9	22.3	23.2	24.1	25.3	26.1
5	5.5	6.9	7.4	8.0	8.7	9.2	21.0	23.7	24.8	25.9	27.3	28.3
6	5.1	6.3	6.8	7.3	8.0	8.4	21.0	23.8	24.9	25.9	27.3	28.3
7	4.3	5.3	5.7	6.1	6.6	7.0	19.0	21.2	22.1	23.0	24.0	24.8
8	5.0	6.1	6.6	7.0	7.6	8.0	19.8	22.2	23.1	24.1	25.3	26.1
9	5.0	6.0	6.5	6.9	7.4	7.8	19.9	22.0	22.8	23.6	24.5	25.3
10	5.3	6.3	6.7	7.1	7.6	8.0	21.3	23.6	24.6	25.5	26.6	27.5
11	4.4	5.3	5.7	6.1	6.6	6.9	18.4	20.4	21.2	21.9	22.9	23.6
12	5.6	6.7	7.2	7.7	8.2	8.7	20.5	22.7	23.5	24.4	25.4	26.2
13	5.5	6.7	7.2	7.7	8.3	8.8	21.4	24.1	25.2	26.3	27.6	28.6
14	6.7	8.0	8.5	9.0	9.7	10.2	20.8	23.2	24.1	25.0	26.1	27.0
15	6.9	8.2	8.8	9.3	10.0	10.5	21.2	23.7	24.6	25.5	26.7	27.5
16	5.2	6.5	7.0	7.5	8.1	8.6	19.3	21.6	22.6	23.5	24.6	25.5

the wave shape parameter at any location. Another interesting consideration is that the point 5 is that characterized by the highest variability of both wind and wave return values. Lastly, from a comparison between wind and wave results it is seen that the point with the highest return values of wind speed does not coincide with the point with the highest return values of significant wave height, which are points 13 and 15, respectively.

4.2. Wind and wave power assessment

This subsection deals with the wind and wave energy characteristics among the examined points. A first estimation concerns the average power at each site calculated from the available data. Specifically, for the wave case it is calculated starting from the estimation of the power associated with each sea state via Equation (11) and then taking the

Table 4
Average wind and wave power.

Point	P_{wave} [kw/m]	P_{wind}[kw/m^2]
1	3.3	0.20
2	2.3	0.25
3	3.7	0.24
4	4.1	0.22
5	4.2	0.22
6	3.2	0.22
7	2.6	0.20
8	4.0	0.20
9	4.1	0.28
10	4.8	0.31
11	3.0	0.19
12	5.3	0.29
13	4.7	0.24
14	9.7	0.28
15	10.0	0.29
16	3.7	0.20

average value. With the same logic but using Equation (20) the power associated to each wind state is estimated and then the average value is calculated. Results of this computation for each considered point are summarized in Table 4.

From the analysis of the average power it is evident that the point at which the maximum wave power and wind power are observed do not coincide. In particular, the most energetic site for what concerns wave energy is represented by the west coast of Sardinia (Points 14 and 15), while the wind most energetic site is Calabria at point 10. Further, it can be observed that as for the analysis of extreme values, the variability of wave power among the considered points is greater than the variability of wind power. More precisely, the wind power variability is about 47% while for the wave power is about 163%, that is about 3.5 times greater. This result reveal that the wind resource is distributed more homogeneously along the considered sites.

After this first calculation the available and useable energy in one year together with operation time are estimated at each point. For this calculation reasonable thresholds have to be considered to define the operational range of a potential wind and wave device. Specifically, for wave energy converted deployed in Mediterranean Sea a cut in and cut out significant wave height values ca be 1 m and 4.5 m, respectively. For what concerns offshore wind turbines, they are characterized by a wind speed operational range that is defined by a cut in wind speed of 5 m/s and a cut out value of 25 m/s. Fig. 5 shows available annual energy in conjunction with annual useable energy and associated operation time, estimated accordingly to the thresholds mentioned above. Further, the percentage of useable energy and operation time with respect to the available ones is listed in the same table.

From Fig. 5 analogous conclusion of those extrapolated from average power can be developed. The useable annual power follows the same trend of annual available power. Among the considered points it is more variable for the wave resource with respect to the wind one. The percentage of annual useable energy varies from a minimum of about 82% to a maximum of about 93% for the wave resource and from a minimum of about 94% to a maximum of about 97% for the wind resource. For what concern the percentage of time during which the potential devices are operative, it varies from a minimum of about 21% to a maximum of about 50% for wave resource and from a minimum of about 44% to a maximum of about 59% for the wind resource.

A deeper analysis is proposed in the following involving the storm concept and investigating how the available and useable energy varies with the storm intensity both for actual storm events and associated EES. Results of this computations are summarized in Fig. 6 for the points exhibiting different characteristics, while those whose results are repetitive and similar to each other are collected in Appendix A3 in Figures A1-A3. to facilitate the reading of the manuscript.

Each figure shows the energy of actual storm event (grey dot), the energy of the associated EES (black dot); the average energy associated to actual storm in each class (red square) of storm intensity 1 m wide, the average energy associated to EES in each class (empty red square) of storm intensity 1 m wide. The left panel pertains to the total energy, while the right panel to the useable one. A general consideration is that

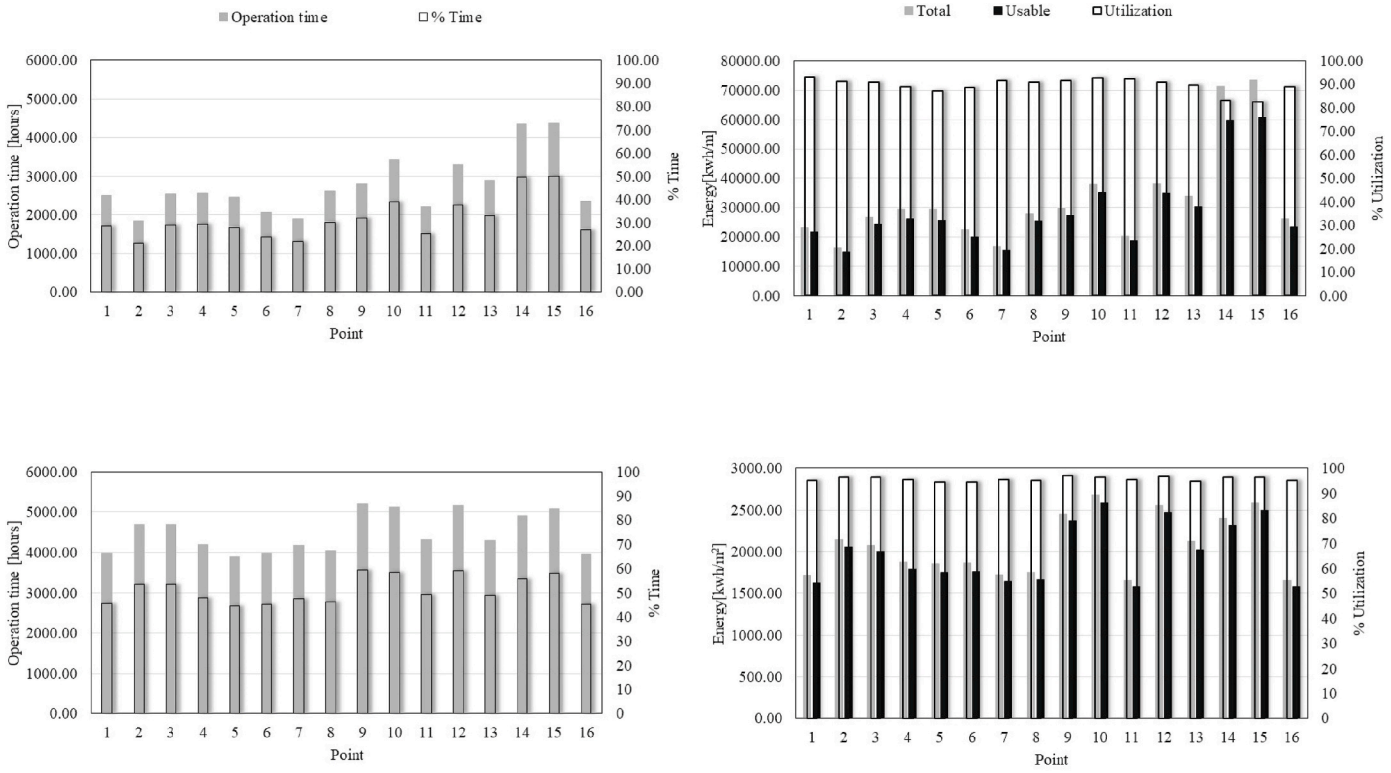

Fig. 5. Operation time (left), available energy and useable energy (right) in a year for wave (top) and wind (bottom) resources.

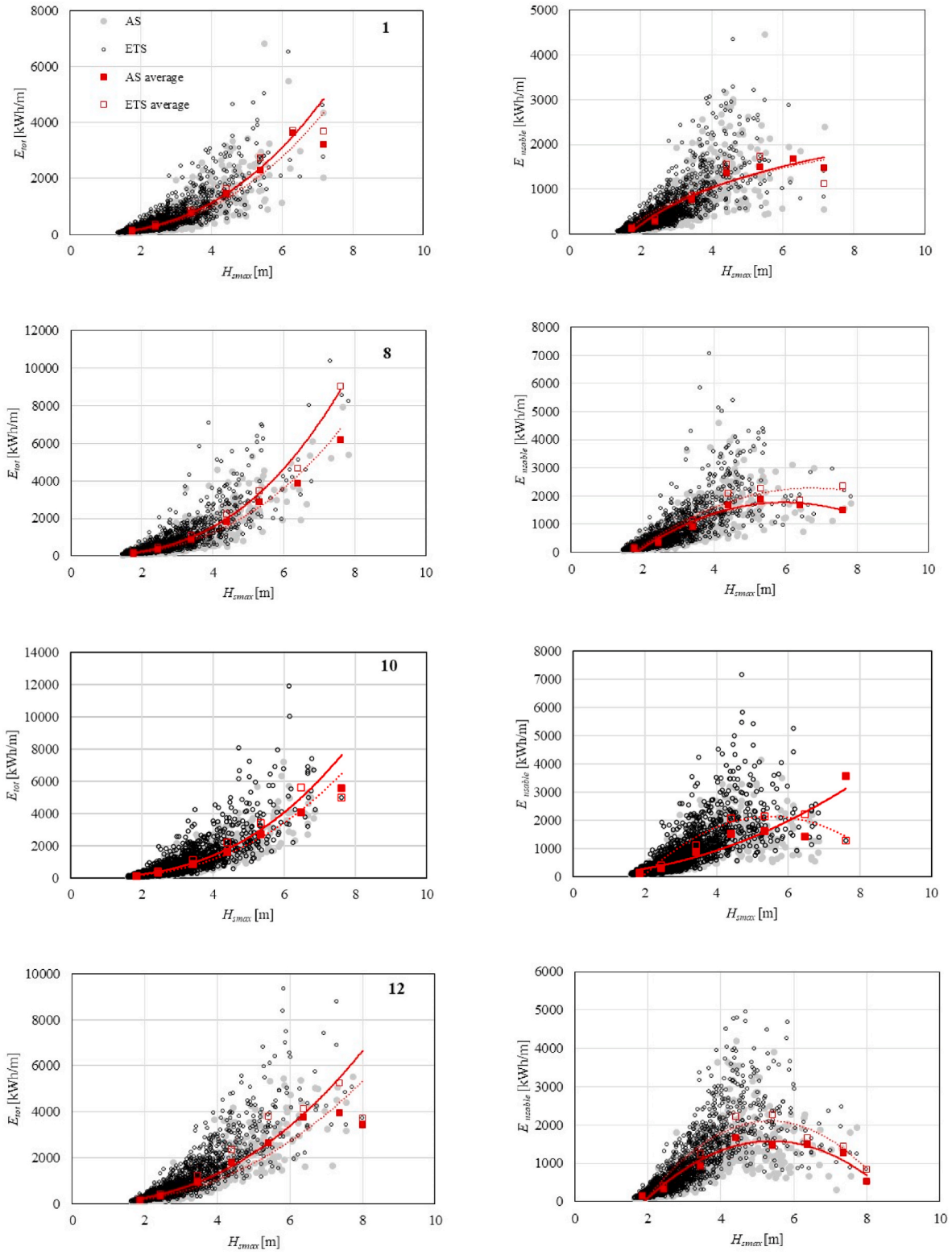

Fig. 6. Total storm energy for AS and EES for all the storms, average for classes of storm intensity of 1 m (left), useable storm energy for AS and EES for all the storms, average for classes of storm intensity of 1 m wide (right) for the points 1, 8, 10, 12.

although there is a statistical equivalence between actual storm and associated EES, the representation of the energy content of the single storm provided by EES model is not good enough neither for total nor for useable energy. However, the average values of these quantities for each class of storm intensity are quite quell represented and in most of the cases they show the same trend by varying the storm intensity. In this regard, it is possible to say that total storm wave energy varies with a power law of the storm intensity H_{smax} for both actual storm and EES. This power law has a form of the type:

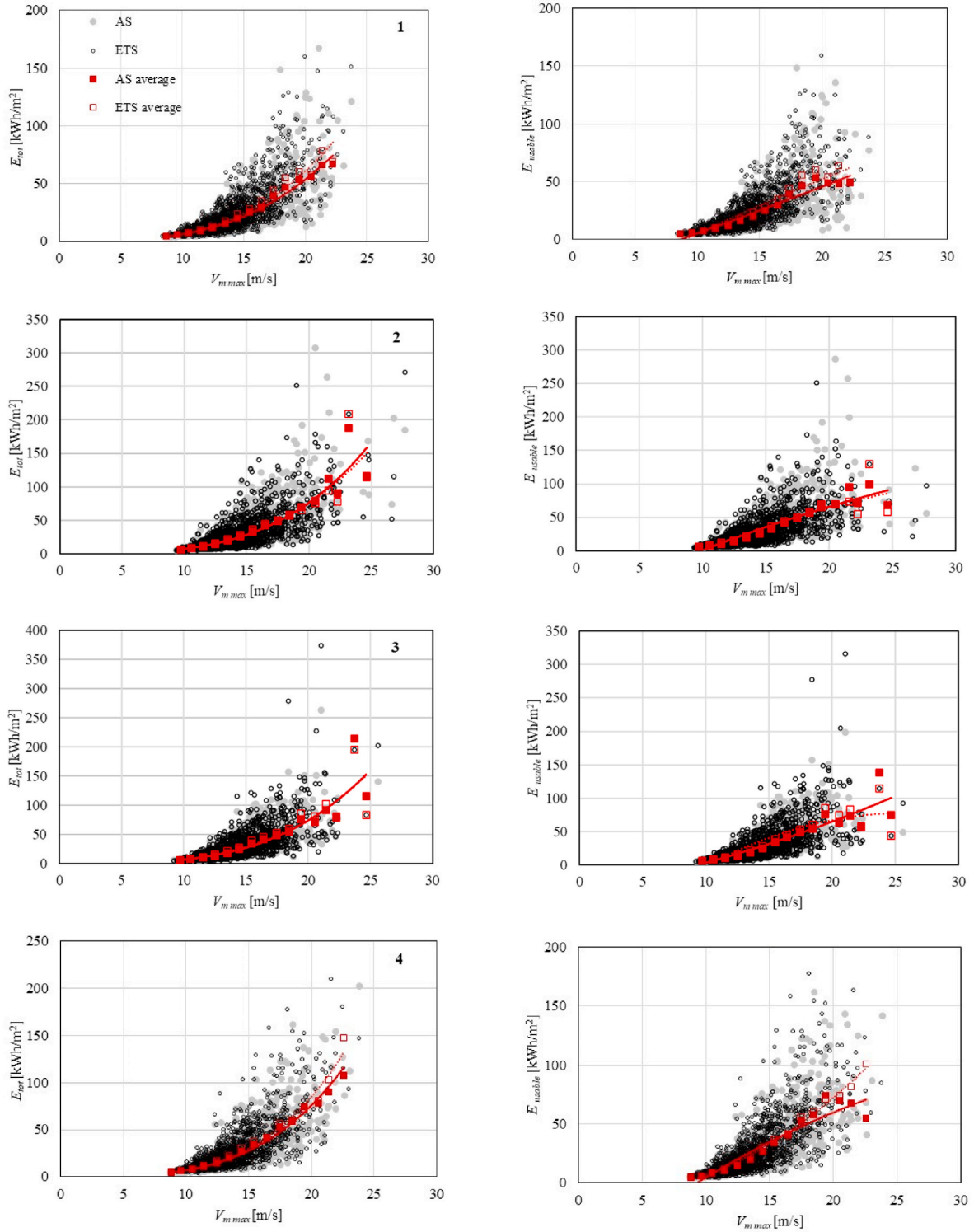

Fig. 7. Total storm energy for AS and EES for all the storms, average for classes of storm intensity of 1 m (left), useable storm energy for AS and EES for all the storms, average for classes of storm intensity of 1 m/s wide (right) from point 1 to point 4.

$$E_{storm}(H_{s\,\max}) = C_1 H_{s\,\max}^{C_2} \tag{24}$$

where coefficients C_1 and exponents C_2 are different from one location to another and for actual storm and EES. However, C_2 is about 2.5 in average while C_1 varies and presents a strong positive correlation with the scale parameter w_{wave} of the location, with a correlation coefficient of 0.75. For the useable energy it is not possible to identify a general law for all the locations. For most of the examined points a logarithmic law is appropriate for both actual storm and EES, but there are some locations e. g. 10 where the behavior of actual storm and EES must be described with different laws. The same analysis has been carried out for wind storm as well and results are represented in Fig. 7 for four representative points. Results for the rest of the points are given in appendix section A3 in Figures A4-A6. For the wind analysis we can draw some different

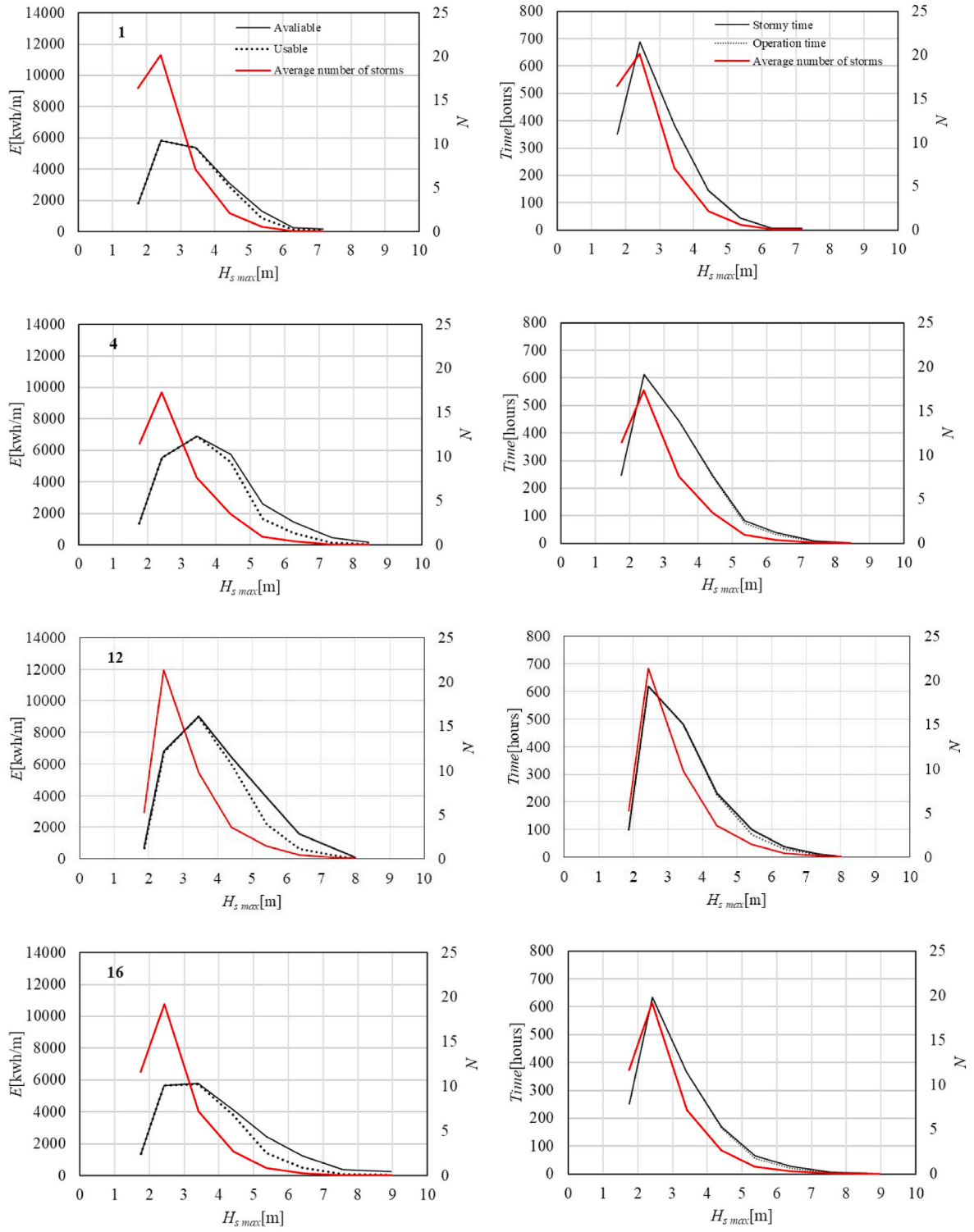

Fig. 8. Wave storm: available and useable wave energy per year for given class of storm intensity H_{smax} (left), stormy time and operation time (right), together with average number of storm events for points 1, 4, 12, 16.

conclusions. A common aspect is that the EES model does not represent adequately the total and useable energy of the single storm event, but the average of total and useable energy of actual storm and EES are in very good agreement. The average of total energy of both actual storm and EES can be fitted by a power law as that of equation (24) for wave case with a power coefficient of about 3 in average. In this case there is no correlation between C_1 factor and scale parameter w_{wind} of wind speed Weibull distribution. The average useable energy of both actual storm and EES can be fitted by a polynomial law.

A further analysis is carried out considering only actual storm data. It

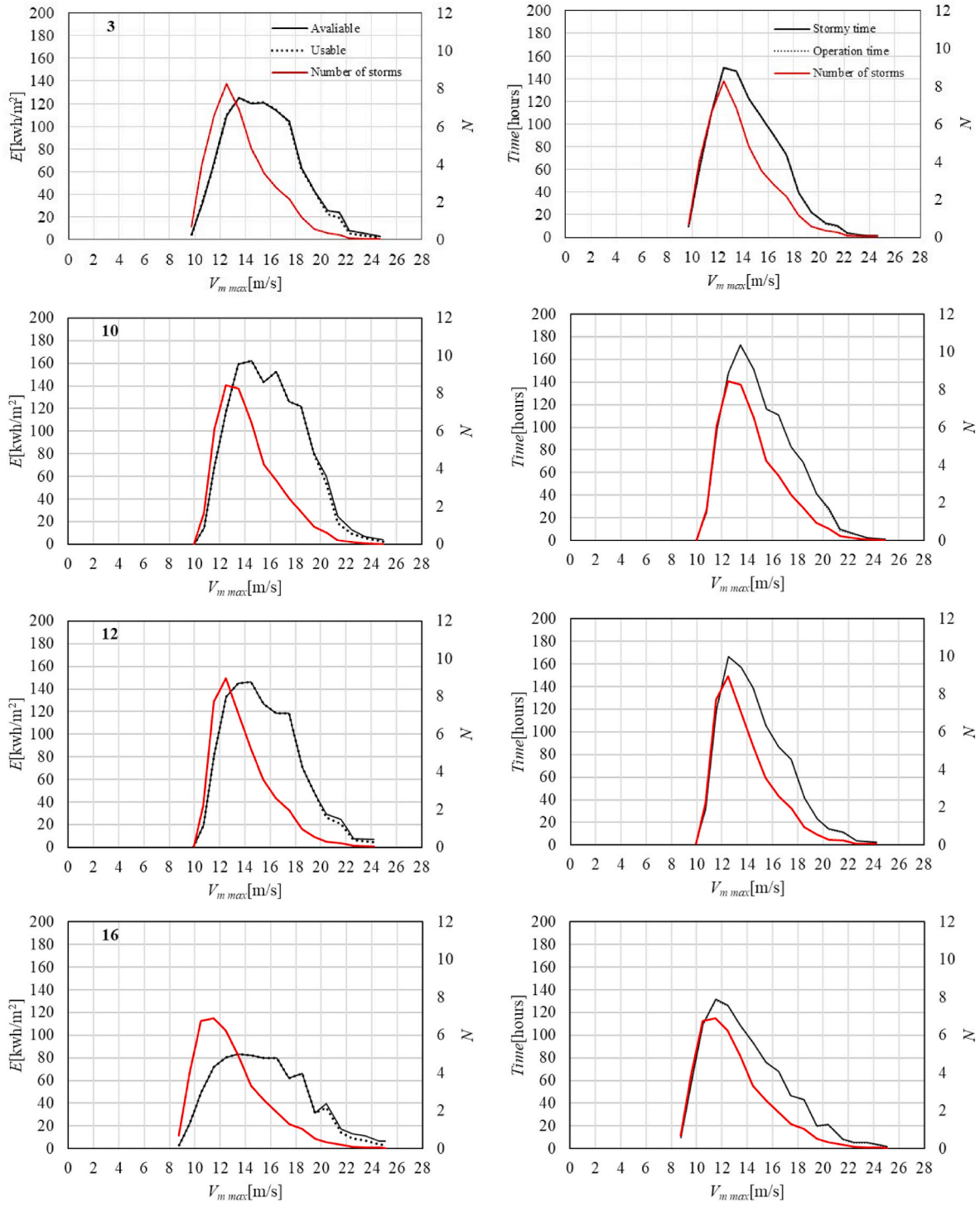

Fig. 9. Wind storm: available and useable wave energy per year for given class of storm intensity $V_{m\,max}$ (left), stormy time and operation time (right), together with average number of storm events for points 3, 10, 12, 16.

consists on the calculation of cumulated total and useable storm energy in a year for given classes of storm intensity, related average number of storm event per year and total cumulated operation time. Results are summarized in Fig. 8 for the wave storm and in Fig. 9 for the wind storm, for the most representative points (see Appendix A3 for the rest of the points at Figures A7-A9 and Figures A10-A12 for wave and wind analysis, respectively). This kind of investigation allows to identify which are the storm events providing the greatest energetic contribution over the year, how many storms of those one could expect, and which is the related operation time. Further from a comparison between total and useable energy curves it is possible to have a visual evaluation of what is the amount of unusable energy with respect to the available one (area

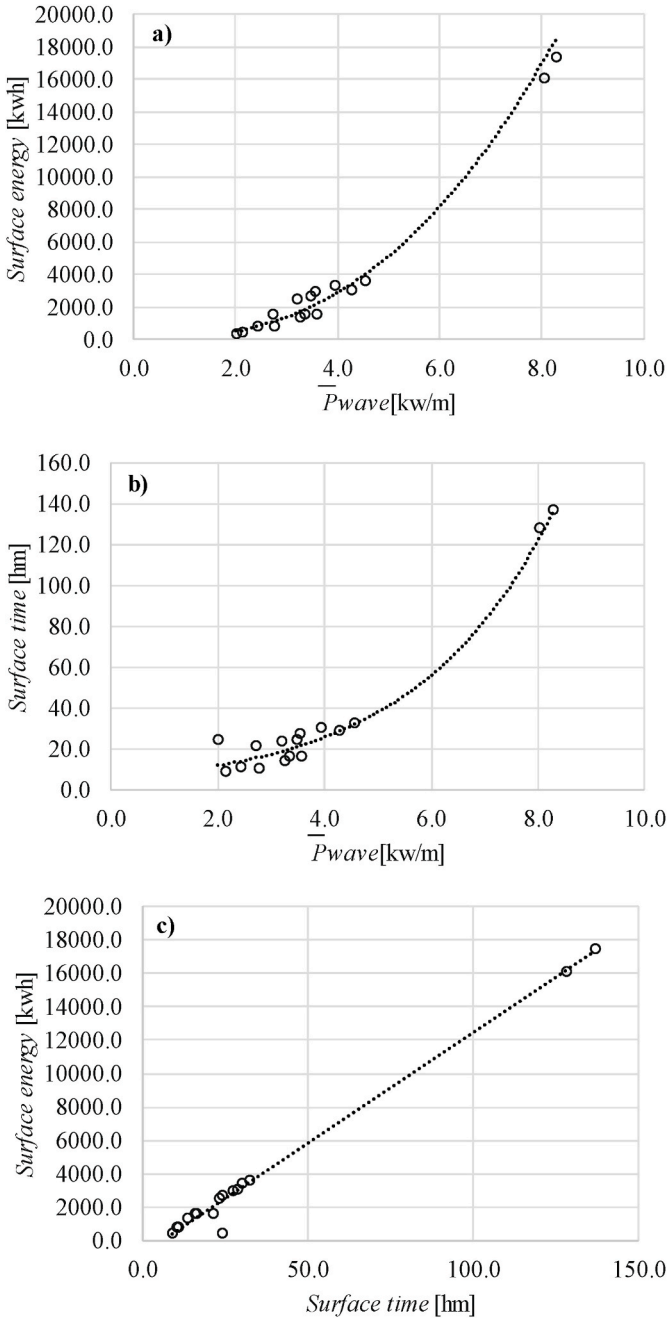

Fig. 10. a) surface between cumulated total and useable energy curves versus average wave power, b) surface between cumulated total and operation time curves versus average wave power, c) surface between total and useable energy curves versus surface between total and operation time curves.

between total and useable energy curves) and in analogy with curves of stormy cumulative time and operation time a measure of downtime can be extrapolated. Fig. 10 gives a more comprehensive information about this aspect. Specifically, from top to bottom it shows the surface between total and useable energy curves versus average wave power at each point (Fig. 10 a), the surface between total stormy and operation time curves versus average wave power at each point (Fig. 10 b), surface between total and useable energy versus surface between total stormy and operation time curves (Fig. 10 c). From the figure it is seen that the amount of unusable power grows with a power law of average wave power at site while the downtime increases exponentially with the average wave power at site. Finally, the amount of unusable energy increases linearly with the downtime.

Table 5
From left to right: average storm peak a_m to which correspond the maximum cumulated storm energy $E_{tot\ cumulated}$ and related average number N_{storm} of storm per year, average storm peak a_m to which correspond the maximum cumulated operation time $T_{op\ cumulated}$ and related average number N_{storm} of storm per year.

Point	a_m[m]	$E_{tot\ cumulated}$ [kwh/m]	Nstorm	a_m[m]	$T_{op\ cumulated}$ [hours]	Nstorm
1	2.4	5812.7	20	2.4	687.5	20
2	2.4	5108.7	18	2.4	690.1	18
3	3.4	6830.0	9	2.4	721.6	22
4	3.4	6919.5	8	2.4	611.6	17
5	3.4	6730.4	7	2.4	665.5	19
6	3.4	5546.5	7	2.4	632.3	18
7	2.4	4459.0	13	2.4	555.0	13
8	2.5	6359.4	19	2.5	660.5	19
9	3.4	6884.7	8	2.4	621.5	19
10	3.4	8672.4	10	2.4	633.8	22
11	2.4	4893.1	15	2.4	583.5	15
12	3.5	8997.8	10	2.4	617.5	21
13	3.4	8359.2	9	2.4	621.7	18
14	4.4	12211.9	7	3.5	516.9	13
15	4.5	12534.9	6	3.4	479.6	12
16	3.4	5765.0	7	2.4	632.2	19

Results of wave analysis show that in most of the examined points (7 over 16, that are 4, 5, 6, 9, 10, 12, 13) the greatest content of total energy comes from the storms with peaks between 3 and 4 m, then there are four locations (1, 2, 7, 11) for which it is between 2 and 3 m and three locations (3, 8, 16) where the contribution of these two classes are comparable. Further, for the most energetic points (14 and 15) pertains to the storms with peak between 4 and 5 m. For what concerns the cumulative operation time, it is seen that its greatest contribution comes from the storms with peak between 2 and 3 m for all the points except for the two most energetic ones (14 and 15) where it is for storm between 3 and 4 m. The above results are summarized in Table 5.

Focusing on the analysis of wind storm energy, the values of storm peaks associated to the maximum cumulative storm energy are more variable from one location to another than for the wave storm case. In particular, for point 7 it is between 11 and 12 m/s, for point 11 between 12 and 13 m/s, for points 3 and 9 between 13 and 14 m/s, for points 1, 2, 8, 14, between 14 and 15 m/s, for point 4 and 13 between 15 and 16 m/s and for points 5, 6 between 16 and 17 m/s. Then there are four points where a wider range can be considered. Specifically, for points 10, 12 it is between 12 and 14 m/s, for point 15 between 13 and 15 m/s and for point 16 between 12 and 17 m/s. For what concerns the cumulative operation time, there are six points (3, 4, 6, 8, 11, 12) where it is maximum for wind storms with peak between 12 and 13 m/s, four points (9, 10, 14, 15) with peak between 13 and 14 m/s, two points (7, 16) with peak between 11 and 12 m/s. In the remaining points it is comparable in a wider range of storm peaks. Specifically, for points (2, 5) it is for storms with peaks between 12 and 14 m/s, for point 1 in 12–16 m/s and for point 13 in 11–15 m/s. In general, one can say that among the analyzed location, the wind storms providing the most energetic cumulative contribution have peaks between 11 and 17 m/s and the greatest cumulative operation time is due to wind storms with peak between 11 and 16 m/s. An important aspect is that with the thresholds selected for the wind operational range the aliquot of energy that cannot

be used is negligible all over the points and the same is observed for the downtimes, obviously. A common feature between wind and wave results, is that the peaks of cumulative total and useable storm energy occurs at the same storm peak values almost at all the points. The same result is achieved by comparing the cumulative total time covered by storm event during the year and cumulative operation time.

5. Conclusions

This paper has proposed a combined wind and wave data analysis focused on extreme value and energy resource assessments in central Mediterranean Sea. Both these two aspects have been investigated mainly from a storm concept perspective. Input data are time series of significant wave height and average wind speed from DICCA MeteOcean database. The extreme value analysis has been focused on the calculation of return values of significant wave height and average wind speed via Equivalent Exponential Storm Model, while resource assessment has involved both simple calculations from data and storm based calculations as well. Results have revealed some interesting information useful for site and technology selection when developing a wind, wave or hybrid farm project over any studied area. In this regard, the correct knowledge of extremes is a key factor of reliability and survivability of the structural part of the involved system, while a correct estimation of available and useable energy, operation time and their variability with storms characteristics help the optimization of the energy converter. The main results have shown that return values of significant wave height are more variable along the considered locations in comparison with those of wind speed, and the location where the severest wave storm occurs differs from that where the severest wind storm occur. In analogy, an analysis of available power has elucidated that the wind power is distributed more homogeneously with respect to the wave power along the considered points, with a relatively lower variability from one location to another. The EES model is not able to describe adequately the energy content of the single storm event but provides a quite good representation of the averages for given classes of intensity giving a correct description on how the total and useable energy of a storm varies with the storm peak. In the case of wind storm the above description tend to coincide with that provided by the actual wind storm sequence. The wave storms providing the greatest cumulated energy contribution among the analyzed points have peaks between 2 and 5 m maximum, while for wind storms peaks are between 11 and 17 m/s. Finally, with the operational range assumed in this for wind and wave devices it is seen that in the wave case there are some locations where a significant amount of available energy cannot be used and this amount grows as the total energy increases. For the wind storm the amount of unusable energy is relatively low everywhere.

Author contribution

Valentina Laface: Conceptualization, Methodology, Software, Formal analysis, Writing. Felice Arena: Methodology, Formal analysis, Writing - Review, Supervision.

Declaration of competing interest

The authors declare that they have no known competing financial interests or personal relationships that could have appeared to influence the work reported in this paper.

Data availability

Data will be made available on request.

Acknowledgements

This work was partially developed in the framework of “The Blue Growth Farm” project (http://www.thebluegrowthfarm.eu/), funded by the European Union’s Horizon2020 research and innovation program (Grant Agreement number 774426). The content of the work does not report the opinion of the European Commission and reflects only the views of the author(s), including errors or omissions. The European Commission is also not liable for any use that may be made of the information contained herein.

The authors are grateful to MeteOcean group of DICCA department of Genoa University for making available the data used in this work.

Appendix A1

As mentioned in exponential storm section, the key point in the development of analytical solutions of the return period of storms with assigned characteristics is related with the derivation of analytical form of probability density function of storm peaks $p_A(a)$, which varies from one model to another (e.g. from triangular to exponential storm model) because is strongly related to the storm shape. Let us consider the wave storm case. For EES model it is determined by imposing that the total time during which the significant wave height is above a given threshold h in a given time interval τ, is the same in actual storm sequence and EES sequence. For actual storm sequence it can be calculated as

$$\tau P(H_s > h) \tag{A1}$$

For the sequence of EES it is calculated as

$$T_{EES}(h) = \int_{a=0}^{\infty} \int_{b=0}^{\infty} N(\tau) p_A(a) p_B(b|a) \delta t(h, h_{crit}, a, b) db da \tag{A2}$$

where $N(\tau)$ is the total number of storms occurring during τ, $p_B(b|a)$ is the probability density function of storm duration b for assigned storm intensity a and $\delta t(h, h_{crit}, a, b)$ is the time interval above the threshold h in an EES with intensity a, duration b, for a location with critical threshold equal to h_{crit}. The time interval $\delta t(h, h_{crit}, a, b)$ is determined by using equation (3), considering the contribution for $t > 0$ multiplied by two (due to storm simmetry with respect to $t = 0$). This time interval is different from zero only for the storms with peak $a > h$ and is given by:

$$\delta t(h, h_{crit}, a, b) = b\frac{\ln\left(\frac{h}{a}\right)}{\ln\left(\frac{h_{crit}}{a}\right)} \tag{A3}$$

Then equating relations (A.1) and (A2) and taking into account that $\delta t(h, h_{crit}, a, b) = 0$ for $a<h$

$$\tau P(H_s > h) = N(\tau)\int_{a=h}^{\infty} p_A(a)\bar{b}(a)\frac{\ln\left(\frac{h}{a}\right)}{\ln\left(\frac{h_{crit}}{a}\right)}da \tag{A4}$$

where $\bar{b}(a) = \int_{b=0}^{\infty} bp_B(b|a)db$ is the intensity-duration regression function.

Finally, the analytical solution of $p_A(a)$ is obtained from equality (A4) deriving twice with respect to h and setting $h = a$.

Note that the same logic is adopted for determining the $p_A(a)$ of wind storm, with the only difference that in this case a represents the wind storm peak and is in m/s.

Appendix A2

For the calculation of $\overline{T}(u)$ the Kaimal spectrum [49] is considered for the wind turbulence

$$S(f) = \frac{4\sigma_k^2 L_k/u}{(1+6fL_k/u)^{5/3}} \tag{A5}$$

where f is the cyclic frequency, u is the mean wind speed, k indicates the direction (1 = longitudinal, 2 = lateral, 3 = vertical), L_k is the turbulence length defined by

$$L_k = \begin{cases} 8.10\Lambda & k=1 \\ 2.70\Lambda & k=2 \\ 0.66\Lambda & k=3 \end{cases} \tag{A6}$$

where Λ is the turbulence scale parameter given by

$$\Lambda = 0.7\ \min(60, \text{hub height}) \tag{A7}$$

Further, in equation (A5) σ_k is the standard deviation of wind turbulence, related to the turbulence intensity I_{ref} that, in turn, depends on the mean wind speed u. For the scope of the calculation of this paper only the longitudinal component is considered and its standard deviation is indicated with σ. Then, introducing the dimensionless frequency $F=(L_k/u)f$, and introducing the dimensionless moments of the spectrum M_0 and M_2:

$$M_0 = \int_0^{\infty} \frac{1}{(1+6F)^{5/3}}\,dF \tag{A8}$$

$$M_2 = \int_0^{\infty} \frac{F^2}{(1+6F)^{5/3}}\,dF \tag{A9}$$

the mean zero up crossing period $\overline{T}(u)$ following Rice approach [50] is expressed as:

$$\overline{T}(u) = 2\pi\,\frac{L_k}{u}\sqrt{\frac{M_0}{M_2}} \tag{A10}$$

Appendix A3

In this appendix the Figures related to the results at points where results are repetitive are grouped.

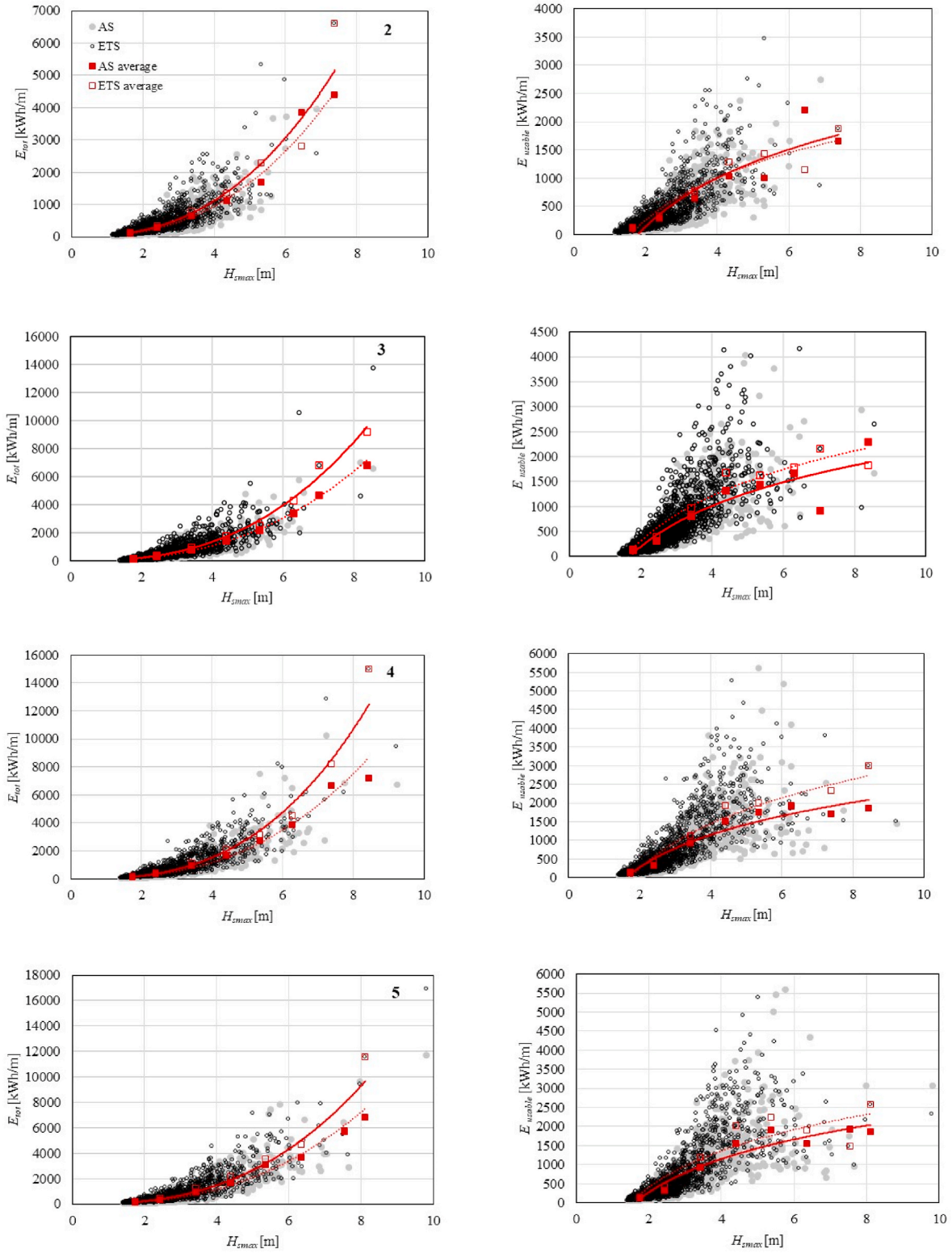

Fig. A1. Total storm energy for AS and EES for all the storms, average for classes of storm intensity of 1 m (left), usable storm energy for AS and EES for all the storms, average for classes of storm intensity of 1 m wide (right) from point 2 to point 5.

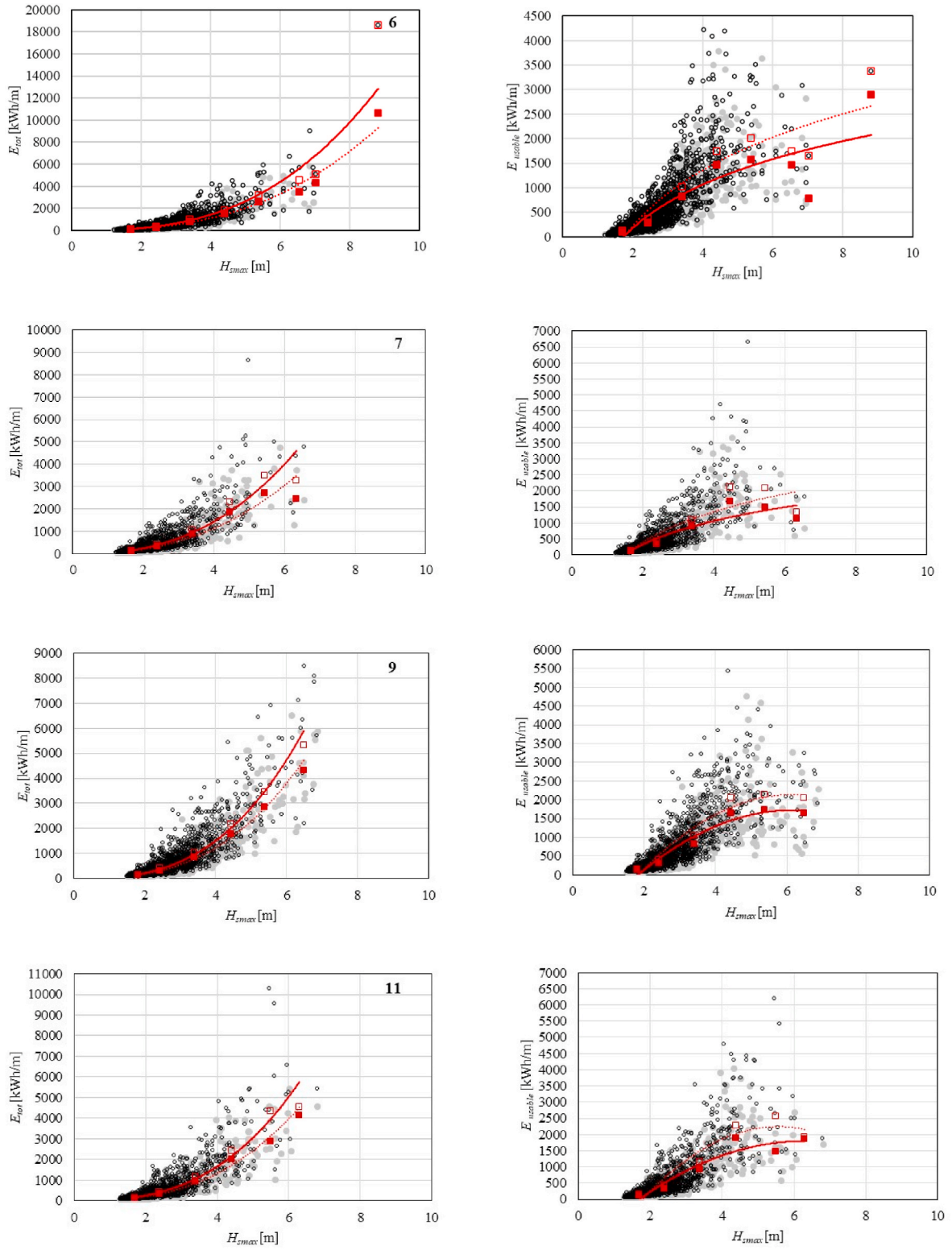

Fig. A2. Total storm energy for AS and EES for all the storms, average for classes of storm intensity of 1 m (left), usable storm energy for AS and EES for all the storms, average for classes of storm intensity of 1 m wide (right) for points 6, 7, 9, 11.

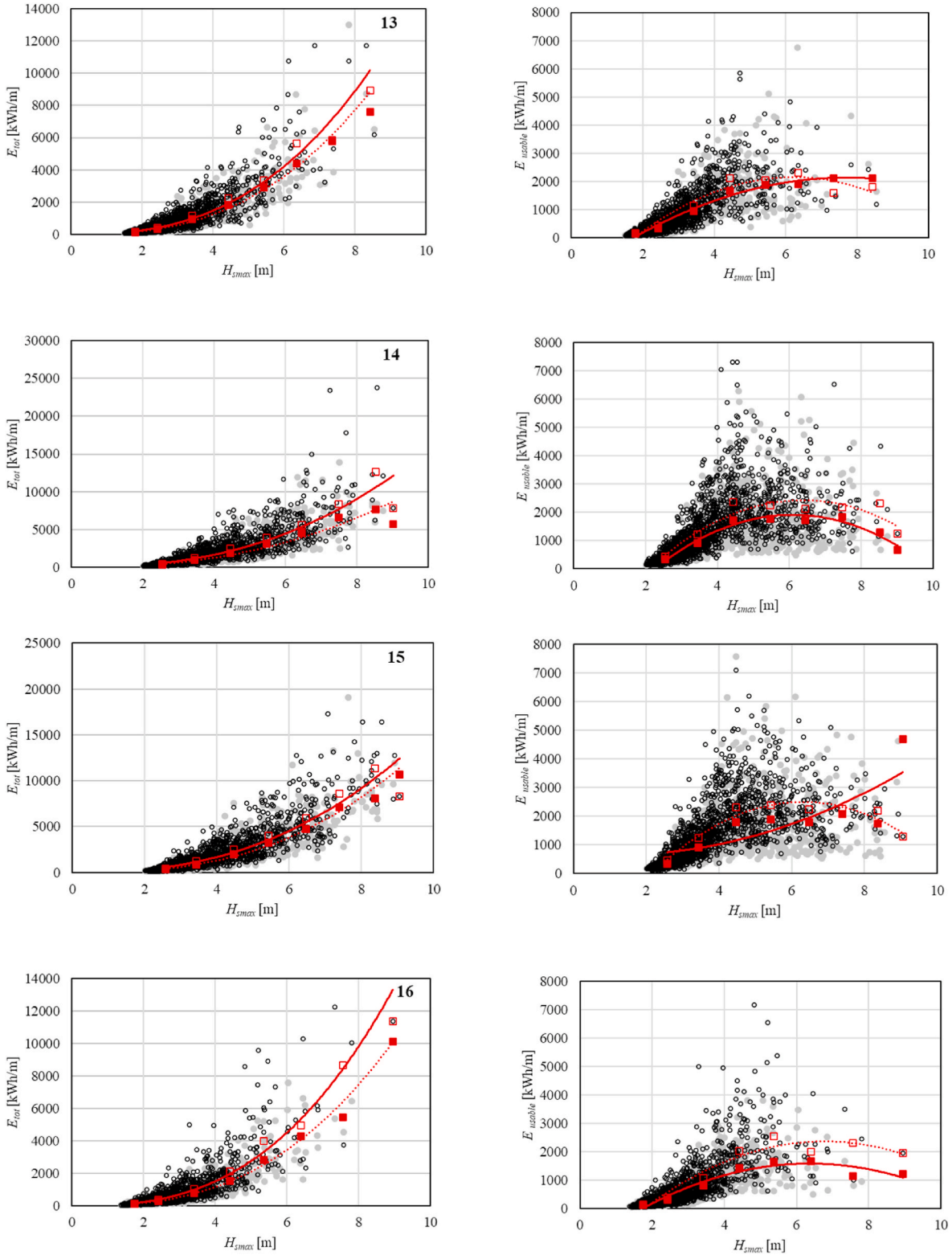

Fig. A3. Total storm energy for AS and EES for all the storms, average for classes of storm intensity of 1 m (left), usable storm energy for AS and EES for all the storms, average for classes of storm intensity of 1 m wide (right) from point 13 to point 16.

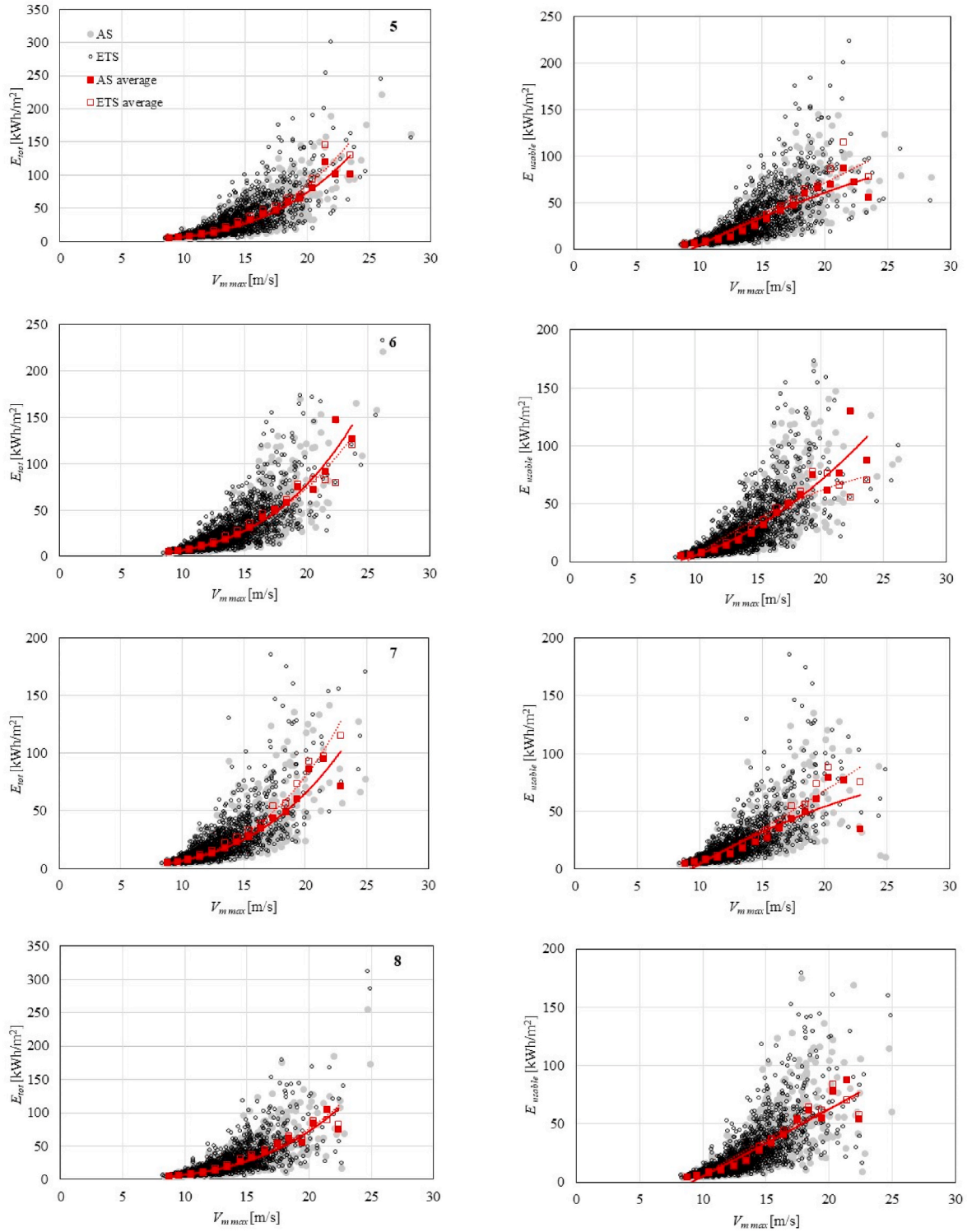

Fig. A4. Total storm energy for AS and EES for all the storms, average for classes of storm intensity of 1 m (left), usable storm energy for AS and EES for all the storms, average for classes of storm intensity of 1 m/s wide (right) from point 5 to point 8.

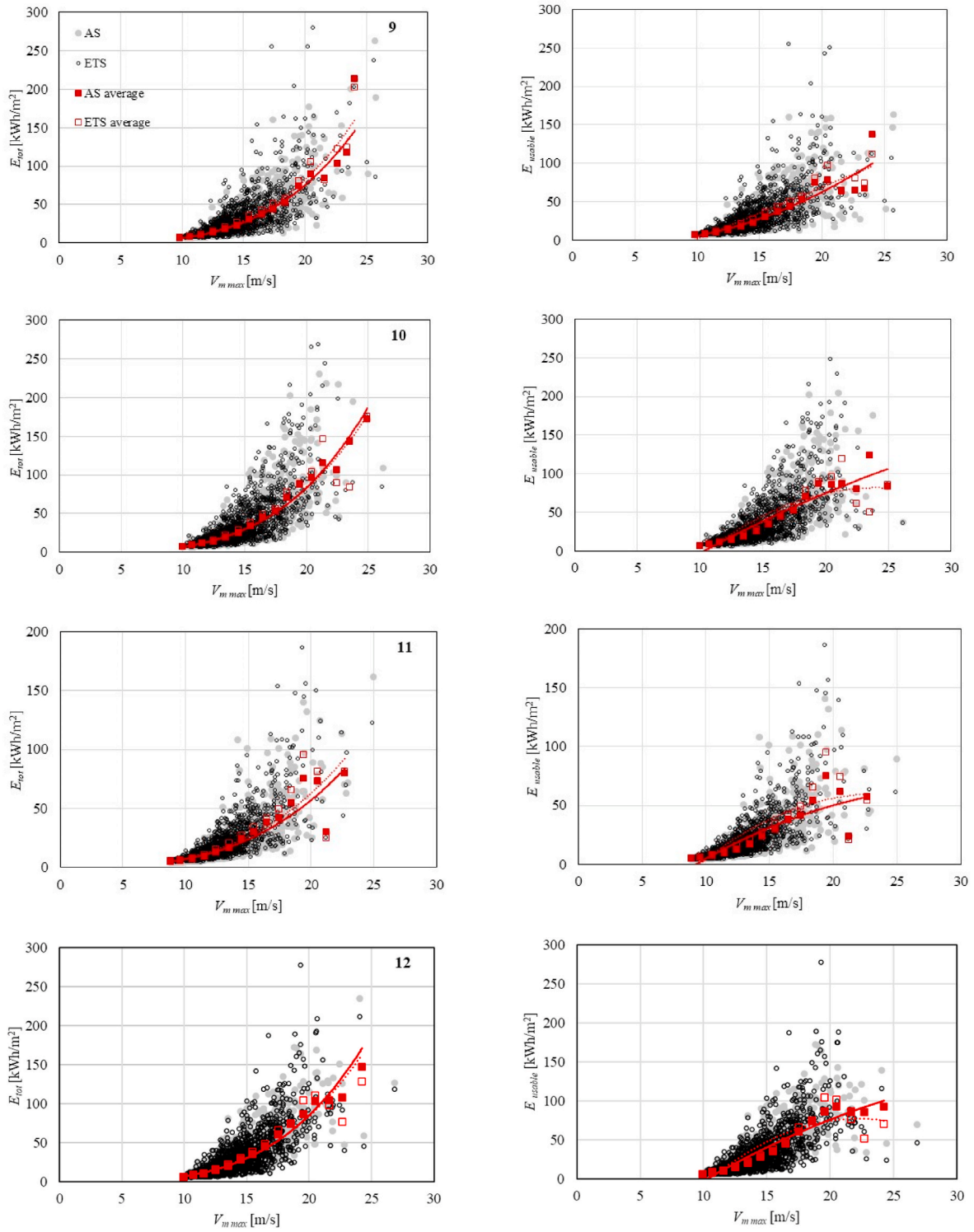

Fig. A5. Total storm energy for AS and EES for all the storms, average for classes of storm intensity of 1 m (left), usable storm energy for AS and EES for all the storms, average for classes of storm intensity of 1 m/s wide (right) from point 9 to point 12.

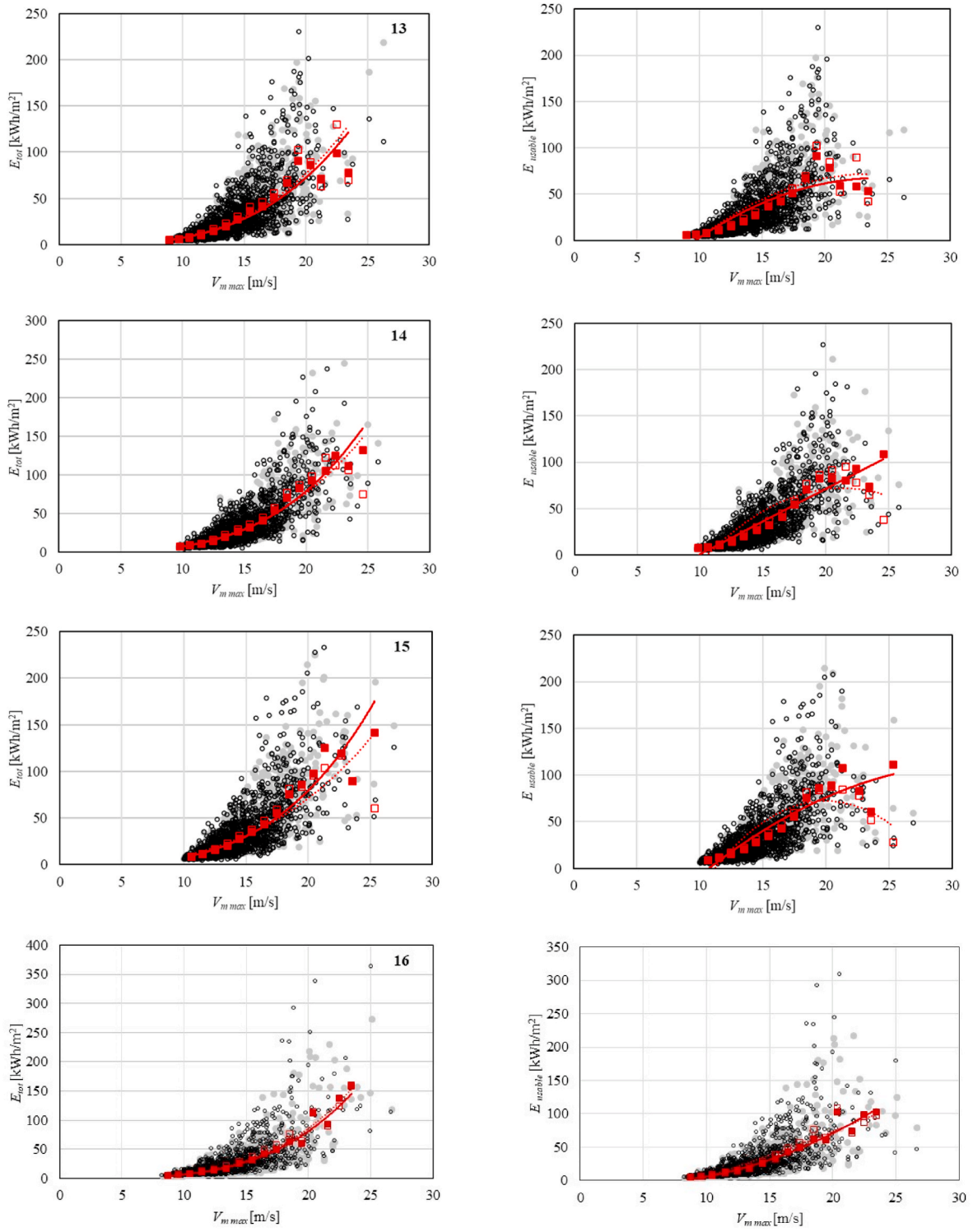

Fig. A6. Total storm energy for AS and EES for all the storms, average for classes of storm intensity of 1 m (left), usable storm energy for AS and EES for all the storms, average for classes of storm intensity of 1 m/s wide (right) from point 13 to point 16.

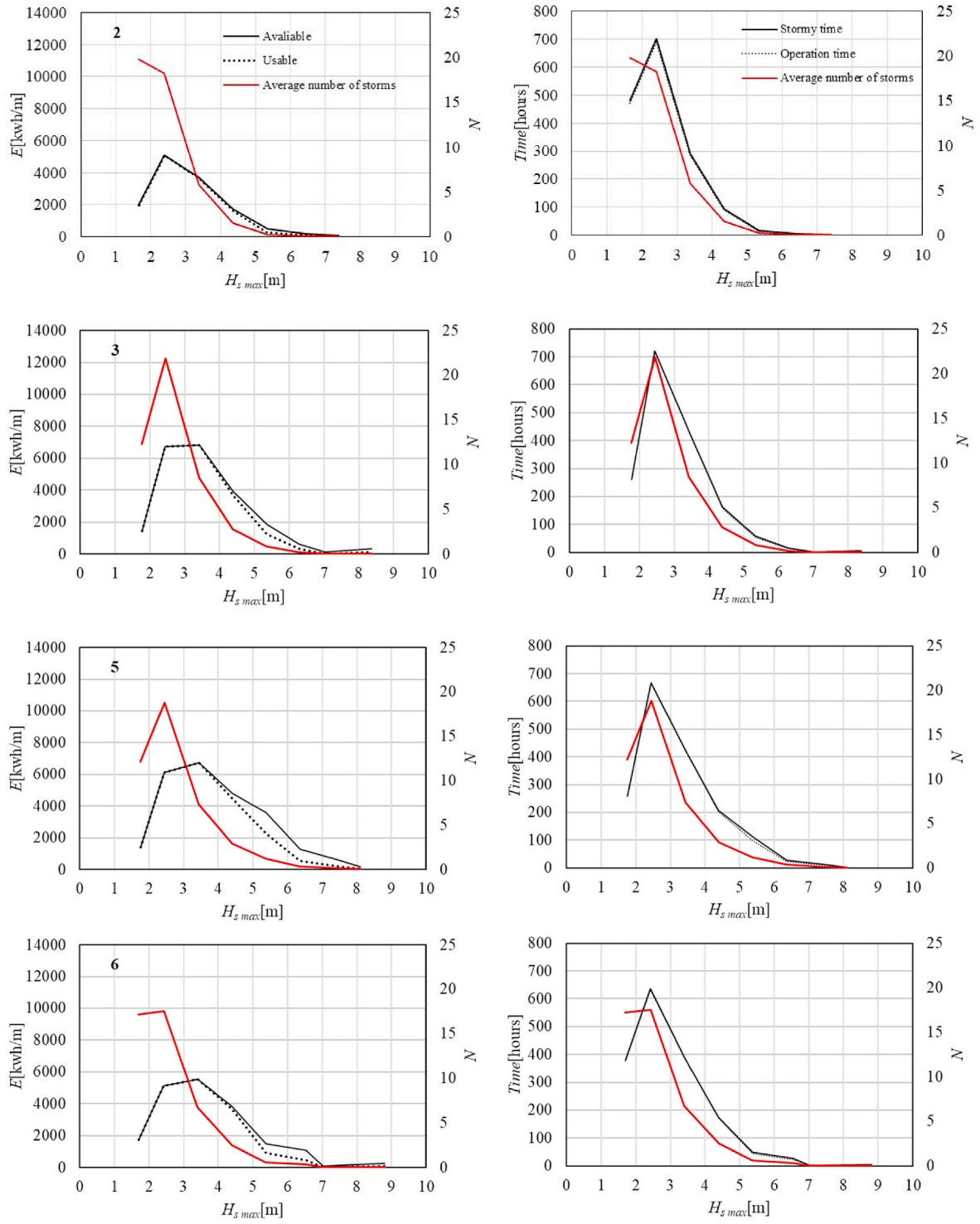

Fig. A7. Wave storm: available and usable wave energy per year for given class of storm intensity H_{smax} (left), stormy time and operation time (right), together with average number of storm events for points 2, 3, 5, 6.

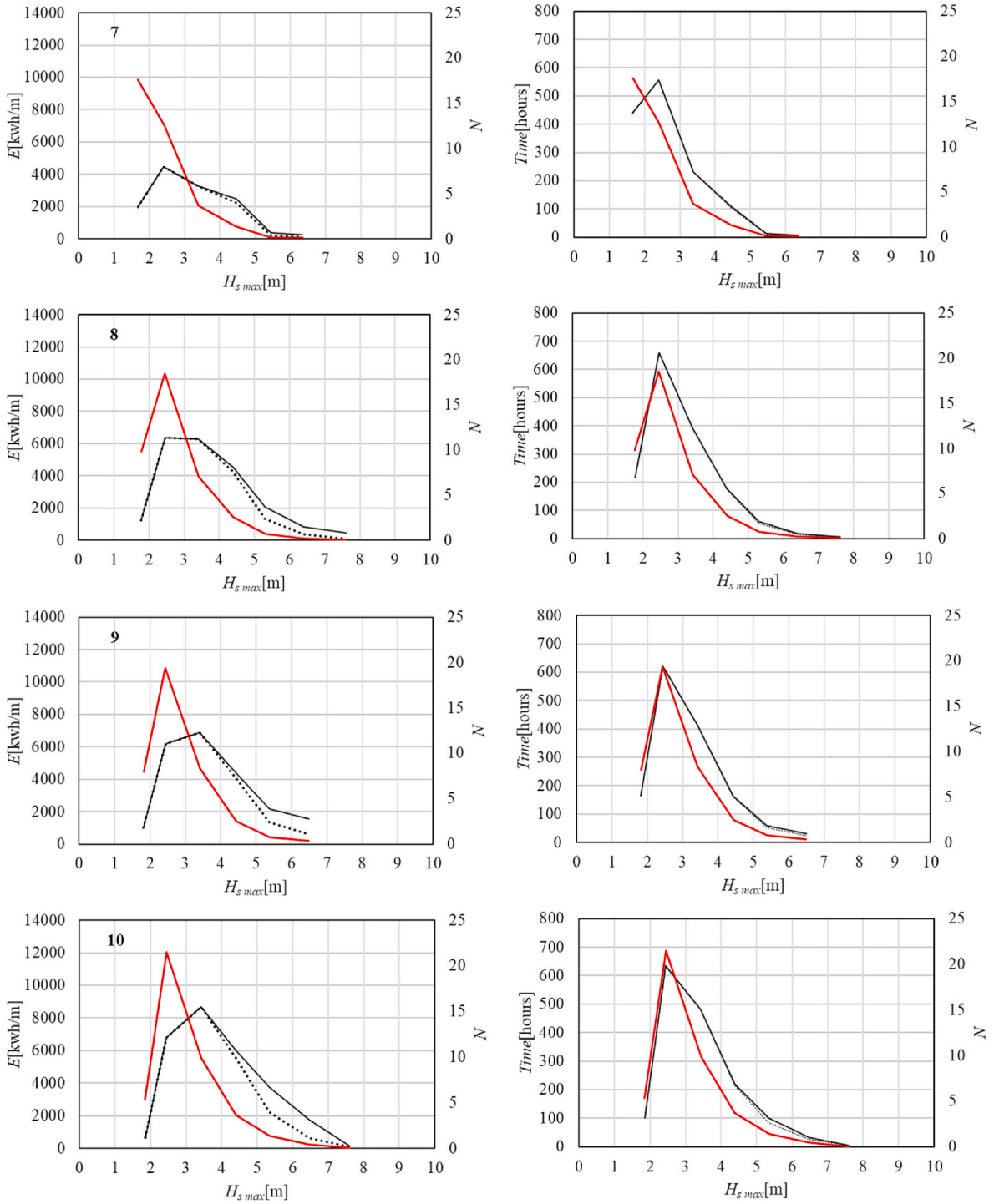

Fig. A8. Wave storm: available and usable wave energy per year for given class of storm intensity H_{smax} (left), stormy time and operation time (right), together with average number of storm events from point 7 to point 10.

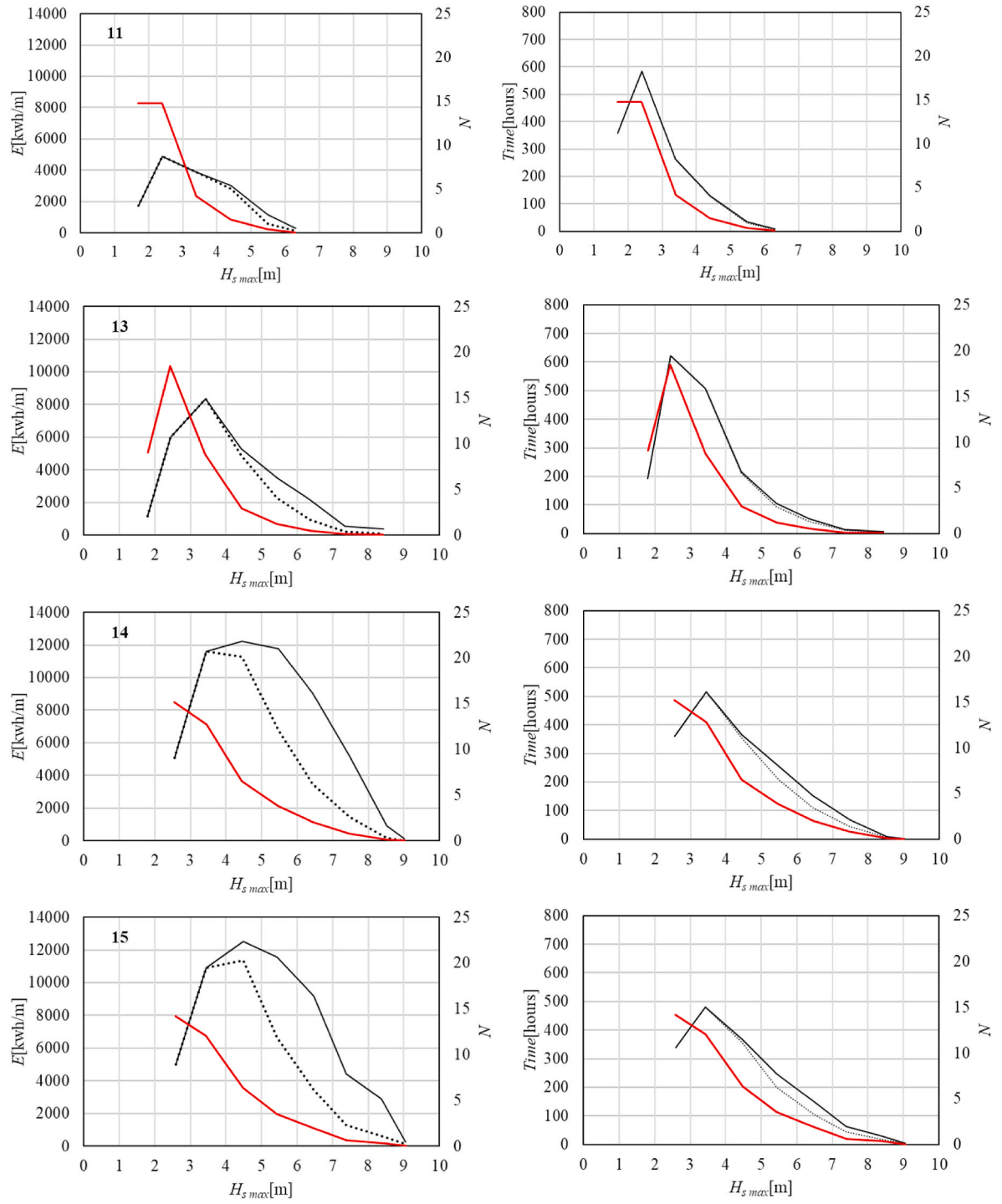

Fig. A9. Wave storm: available and usable wave energy per year for given class of storm intensity H_{smax} (left), stormy time and operation time (right), together with average number of storm events for points 11, 13, 14, 15.

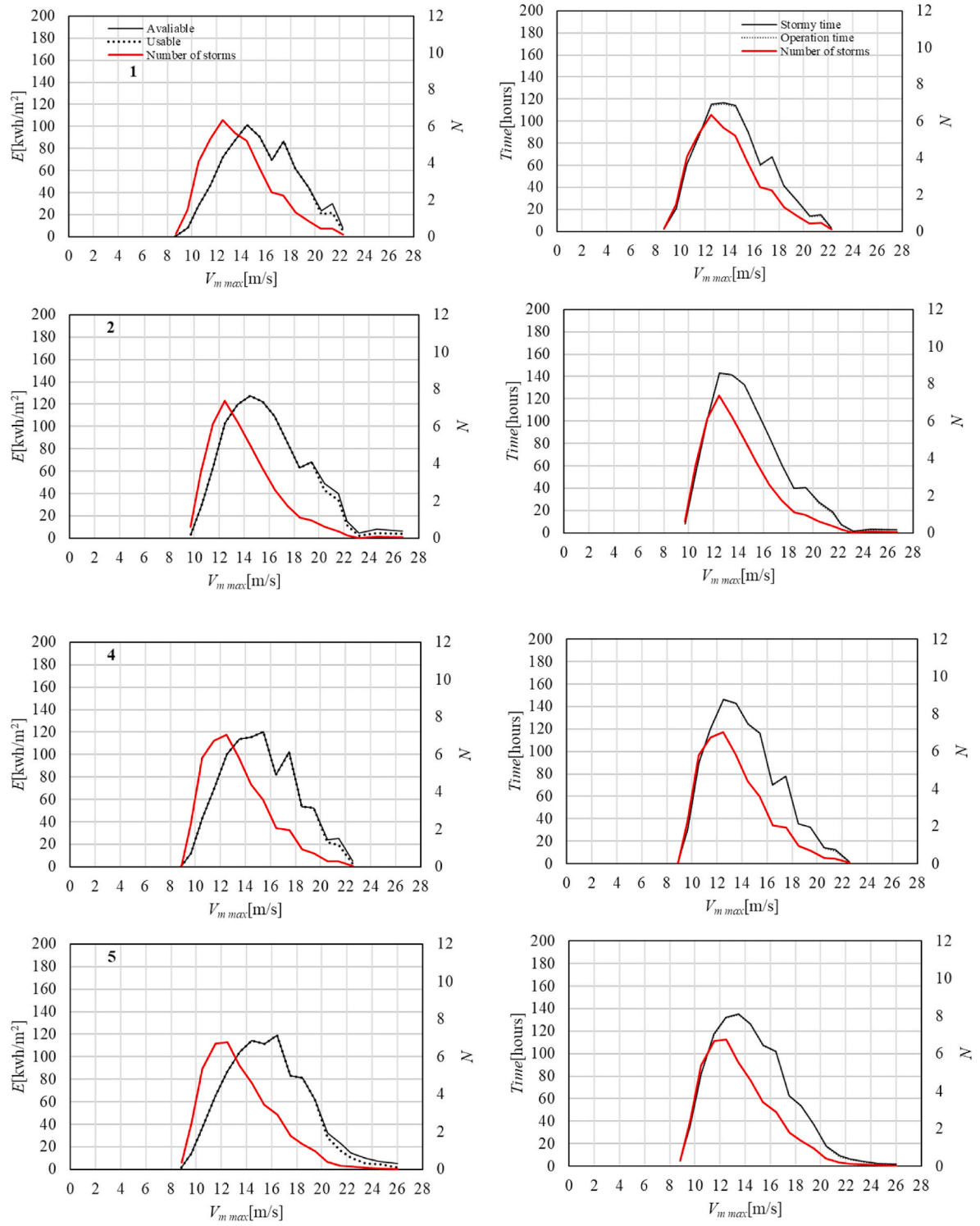

Fig. A10. Wind storm: available and usable wave energy per year for given class of storm intensity $V_{m\,max}$ (left), stormy time and operation time (right), together with average number of storm events for points 1, 2, 4, 5.

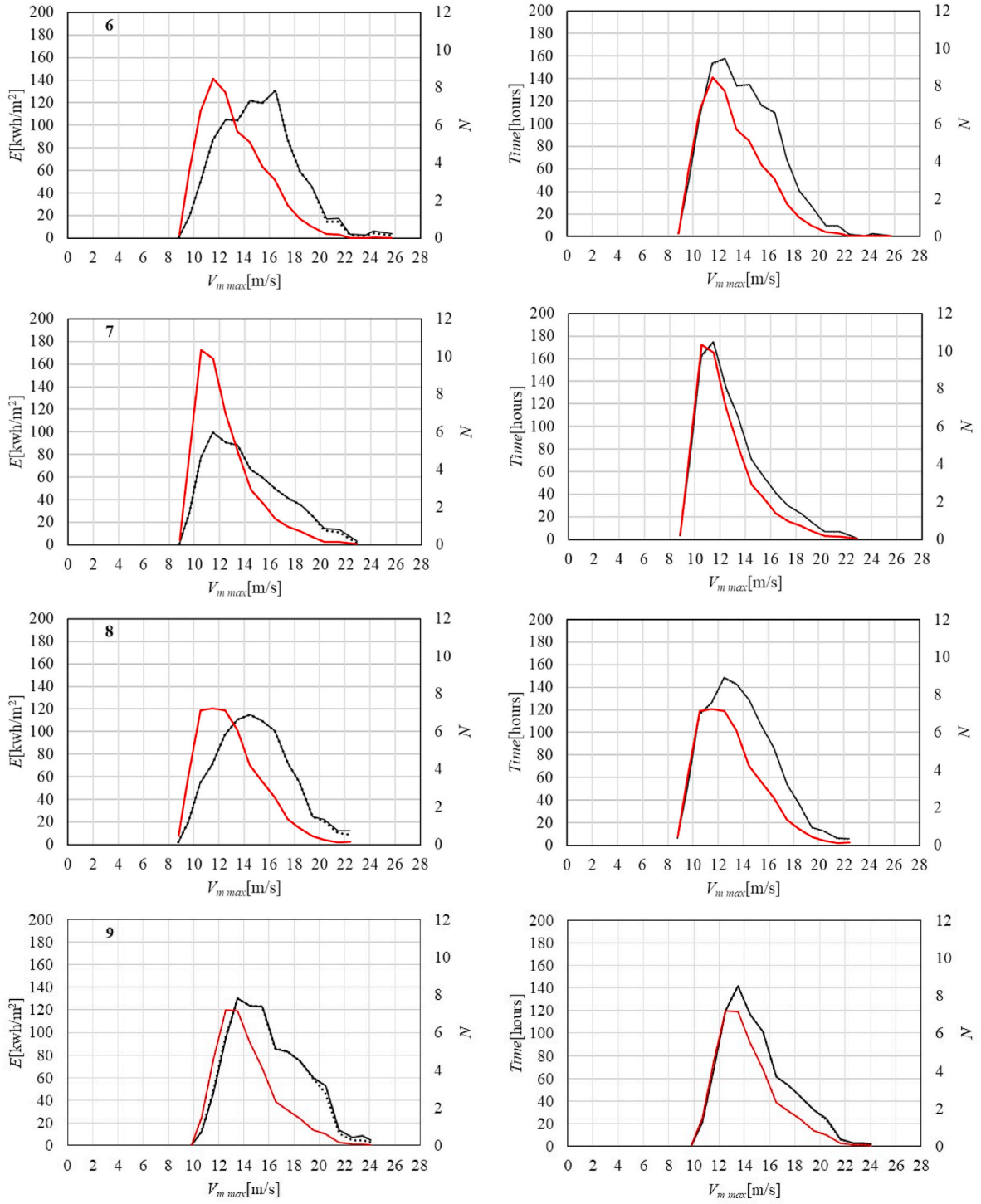

Fig. A11. Wind storm: available and usable wave energy per year for given class of storm intensity $V_{m\,max}$ (left), stormy time and operation time (right), together with average number of storm events from point 6 to point 9.

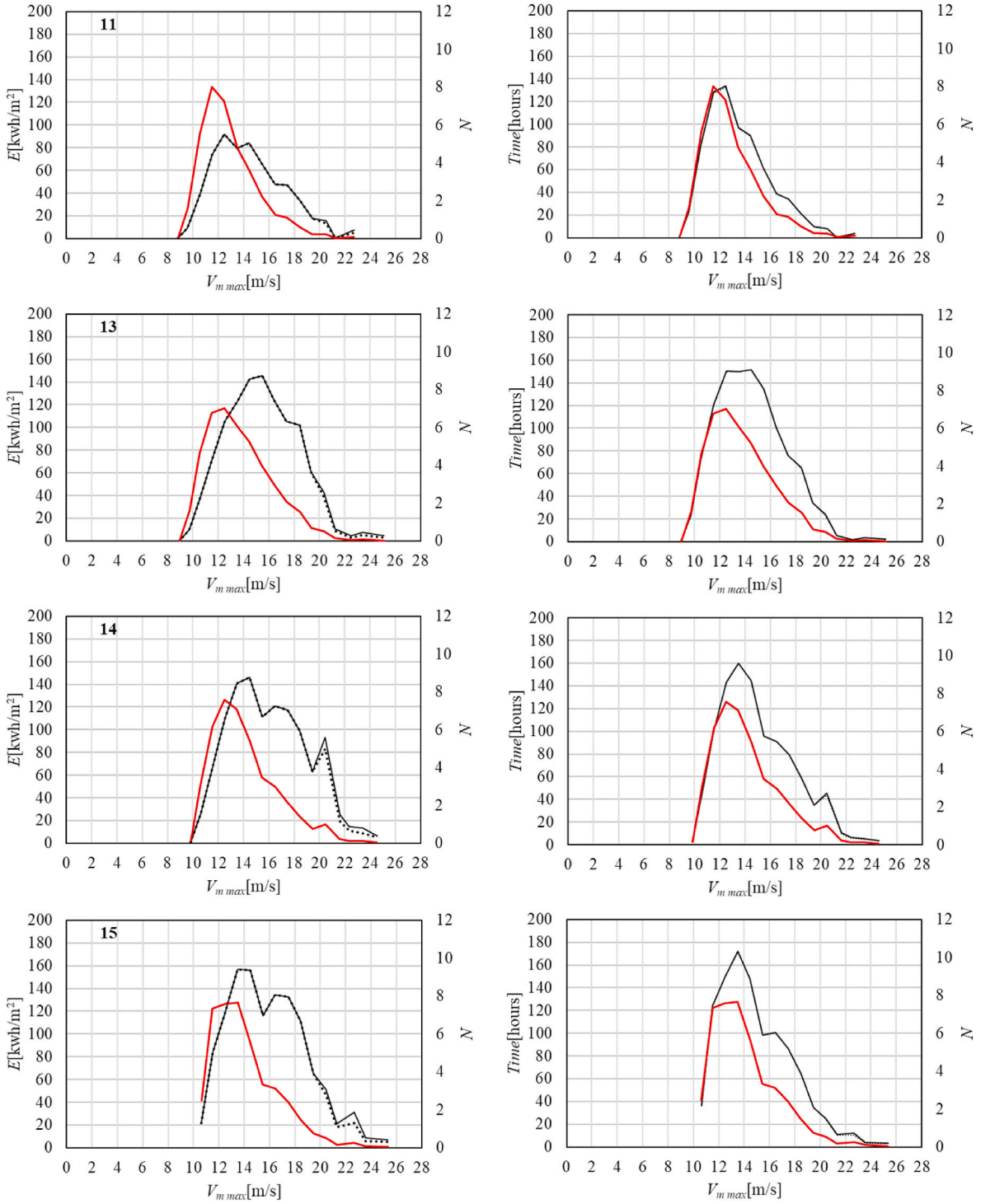

Fig. A12. Wind storm: available and usable wave energy per year for given class of storm intensity $V_{m\ max}$ (left), stormy time and operation time (right), together with average number of storm events for points 11, 13, 14, 15.

References

[1] Schweizer J, Antonini A, Govoni L, Gottardi G, Archetti R, Supino E, Berretta C, Casadei C, Ozzi C. Investigating the potential and feasibility of an offshore wind farm in the Northern Adriatic Sea. Appl Energy 2016;177:449–63. https://doi.org/10.1016/j.apenergy.2016.05.114.

[2] Zountouridou EI, Kiokes GC, Chakalis S, Georgilakis PS, Hatziargyriou ND. Offshore floating wind parks in the deep waters of Mediterranean Sea. Renew Sustain Energy Rev 2015;51:433–48. https://doi.org/10.1016/j.rser.2015.06.027. ISSN 1364-0321.

[3] Maienza C, Avossa AM, Picozzi V, Ricciardelli F. Feasibility analysis for floating offshore wind energy. Int J Life Cycle Assess 2022;27(2022):796–812. https://doi.org/10.1007/s11367-022-02055-8.

[4] Bozzi S, Besio G, Passoni G. Wave power technologies for the Mediterranean offshore: scaling and performance analysis. Coast Eng 2018;136:130–46. https://doi.org/10.1016/j.coastaleng.2018.03.001. ISSN 0378-3839.

[5] Arena F, Fiamma V, Laface V, Malara G, Romolo A, Viviano A, Gianmaria Sannino, Carillo A. Proceedings of the international conference on offshore mechanics and arctic engineering – OMAE. 2013. https://doi.org/10.1115/OMAE2013-10928.

[6] Giuliana M. State of the art and perspectives of wave energy in the Mediterranean Sea: backstage of ISWEC. Front Energy Res 2019;7. https://doi.org/10.3389/fenrg.2019.00114.

[7] Ratsimandresey AW, Sotillo MG, Carretero Albiach JC, Álvarez Fanjul E, Hajji H. A 44-year high-resolution ocean and atmospheric hindcast for the Mediterranean Basin developed within the HIPOCAS Project. 2008 Coast Eng 2008;55(11):827–42. https://doi.org/10.1016/j.coastaleng.2008.02.025. ISSN 0378-3839.

[8] Musić S, Nicković S. 44-year wave hindcast for the Eastern Mediterranean. 2008 Coast Eng 2008;55(Issue 11):872–80. https://doi.org/10.1016/j.coastaleng.2008.02.024. ISSN 0378-3839.

[9] Mentaschi L, Besio G, Cassola F, Mazzino A. Implementation and validation of a wave hindcast/forecast model for the West Mediterrenean. Plymouth, UK Proc of 12th International Coastal Symposium 2013:8–12 [April].

[10] Donatini L, Lupieri G, Contento G, Pedroncini A, Cusati LA, Crosta A. MWM: a 35 years wind&wave high resolution hindcast dataset and an operational forecast service for the mediterranean sea 18th. Int. Conf. Ships Shipp. Res. NAV 2015;2015:116–25. https://arts.units.it/handle/11368/2919934#.XBd8tGko_IU.

[11] Barbariol F, Davison S, Falcieri FM, Ferretti R, Ricchi A, Sclavo M, A, Benetazzo A. Wind waves in the Mediterranean Sea: an ERA5 reanalysis wind-based climatology. Front Mar Sci 2021. https://doi.org/10.3389/fmars.2021.760614. 16 November 2021 Sec. Physical Oceanography.

[12] Liberti L, Carillo A, Sannino G. Wave energy resource assessment in the Mediterranean, the Italian perspective. Renew Energy 2013;50:938–49. https://doi.org/10.1016/j.renene.2012.08.023. ISSN 0960-1481.

[13] Arena F, Laface V, Malara G, Romolo A, Viviano A, Fiamma V, Sannino A, Carillo A. Wave climate analysis for the design of wave energy harvesters in the Mediterranean Sea. Renew Energy 2015;77:125–41. https://doi.org/10.1016/j.renene.2014.12.002. ISSN 0960-1481.

[14] Besio G, Mentaschi L, Mazzino A. Wave energy resource assessment in the Mediterranean Sea on the basis of a 35-year hindcast. Energy 2016;94(2016):50–63. https://doi.org/10.1016/j.energy.2015.10.044. ISSN 0360-5442.

[15] Amarouche K, Akpınar A, Bachari NEI, Houma F. Wave energy resource assessment along the Algerian coast based on 39-year wave hindcast. Renew Energy 2020;153:840–60. https://doi.org/10.1016/j.renene.2020.02.040.

[16] Lavagnini A, Sempreviva AM, Transerici C, Accadia C, Casaioli M, Mariani S, et al. Offshore wind climatology over the Mediterranean basin, vol. 9. Wind Energy; 2006. p. 251–66.

[17] Soukissian T, Karathanasi F, Axaopoulos P. Satellite-based offshore wind resource assessment in the Mediterranean Sea. Ieee J Oceanic Eng 2017;42:73–86. https://doi.org/10.1109/JOE.2016.2565018.

[18] Görmüş T, Aydoğan B, Ayat B. Offshore wind power potential analysis for different wind turbines in the Mediterranean Region, 1959–2020. Energy Convers Manag 2022;274:116470. https://doi.org/10.1016/j.enconman.2022.116470. ISSN 0196-8904.

[19] Ferrari F, Besio G, Cassola F, Mazzino A. Optimized wind and wave energy resource assessment and offshore exploitability in the Mediterranean Sea. 2020 Energy 2020;190:116447. https://doi.org/10.1016/j.energy.2019.116447. ISSN 0360-5442.

[20] Azzellino A, Lanfredi C, Riefolo L, De Santis V, Contestabile P, Vicinanza D. Combined exploitation of offshore wind and wave energy in the Italian seas: a spatial planning approach. Front Energy Res 2019;7. https://doi.org/10.3389/fenrg.2019.00042.

[21] Kalogeri C, Galanis G, Spyrou C, Diamantis D, Baladima F, Koukoula M, Kallos G. Assessing the European offshore wind and wave energy resource for combined exploitation. Renew Energy 2017.

[22] Ganea D, Amortila V, Mereuta E, Rusu E. A joint evaluation of the wind and wave energy resources close to the Greek islands. Sustainability 2017;9:1025.

[23] De Leo F, Solari S, Besio G. Extreme wave analysis based on atmospheric pattern classification: an application along the Italian coast. Nat Hazards Earth Syst Sci 2020;20(2020):1233–46. https://doi.org/10.5194/nhess-20-1233-2020.

[24] Sartini L, Besio G, Cassola F. Spatio-temporal modelling of extreme wave heights in the Mediterranean Sea. Ocean Model 2017;117:52–69.

[25] Sotillo MG, Aznar R, Valero F. Mediterranean offshore extreme wind analysis from the 44-year HIPOCAS database: different approaches towards the estimation of return periods and levels of extreme values. Adv Geosci 2006;7:275–8. https://doi.org/10.5194/adgeo-7-275-2006.

[26] Vinoth J, Young IR. Global estimates of extreme wind speed and wave height. J Clim 2011;24(6):1647–65. http://www.jstor.org/stable/26190457.

[27] Lionello P, Malanotte P, Rizzoli Boscolo R, Alpert P, Artale V, Li L, Luterbacher J, May W, Trigo R, Tsimplis M, Ulbrich U, Xoplaki E. In: Lionello P, Malanotte-Rizzoli, Boscolo R, editors. The Mediterranean climate: an overview of the main characteristics and issues P. Mediterranean, vol. 4. Elsevier; 2006. p. 1–26. https://doi.org/10.1016/S1571-9197(06)80003-0. 2006.

[28] Kapelonis ZG, Gavriliadis PN, Athanassoulis GA. Extreme value analysis of dynamical wave climate projections in the Mediterranean Sea. Procedia Comput Sci 2015;66(2015):210–9. https://doi.org/10.1016/j.procs.2015.11.025. ISSN 1877-0509.

[29] Laface V, Arena F. A new equivalent exponential storm model for long-term statistics of ocean waves. Coast Eng 2016;116:133–51. https://doi.org/10.1016/j.coastaleng.2016.06.011. CENG3144.

[30] Boccotti P. Wave mechanics and wave loads on marine structures. Amsterdam: Butterworth-Heinemann, Elsevier; 2014.

[31] Fedele F, Arena F. The equivalent power storm model for long-term predictions of extreme wave events. J Phys Oceanogr 2010;40:1106–17.

[32] Laface V, Bitner-Gregersen E, Arena F, Romolo A. A parameterization of DNV-GL storm profile for the calculation of design wave of marine structures. Mar Struct 2019;68. https://doi.org/10.1016/j.marstruc.2019.102650.

[33] Mackay E, Johanning J. A generalised equivalent storm model for longterm statistics of ocean waves. Coast Eng 2018;140:411–28.

[34] Tendijck, Ross E, Randell D, Jonathan P. A non-stationary statistical for the evolution of extreme storm events. Environmetrics 2019;30:e2541.

[35] Tendijck P Jonathan D Randell, Tawn J. Temporal evolution of the extreme excursions of multivariate kth order Markov processes with application to oceanographic data. https://arxiv.org/abs/2302.14501; 2023.

[36] Winter HC, Tawn JA. Modelling heatwaves in central France: a casestudy in extremal dependence. J Roy Stat Soc C 2016;65:345–65.

[37] Borgman LE. Maximum wave height probabilities for a random number of random intensity storms. Proc. 12th conf. Coastal eng, vol. 1970. Washington, DC: ASCE; 1970. p. 53–64.

[38] Borgman LE. Probabilities for highest wave in hurricane. J Waterw Harbors Coast Eng Div Amer Soc Civ Eng 1973;99:185–207.

[39] Arena F, Guedes Soares C, Petrova P. Theoretical analysis of average wave steepness related to Peak Period or to Mean Period. In: Proceedings of of the ASME 2010 29th international conference on ocean. Shanghai, China: Offshoreand Arctic Engineering; 2010. 6-11 June 2010.

[40] Laface V, Arena F. On correlation between wind and wave storms. J Mar Sci Eng 2021;9(12):1426. https://doi.org/10.3390/jmse9121426.

[41] Powell David C, Connell James R. Definition of gust model concepts and Review of gust models. Prepared for the U.S. Department of Energy under; 1980. Contract DE-AC06-76RLO 1830.

[42] Laface V, Arena F, Romolo A. Storm models for the calculation of extreme wind speed. Proceedings of the ASME 2022 41st International Conference on Ocean, Offshore and Arctic EngineeringOMAE2022-81323 2022:7. https://doi.org/10.1115/OMAE2022-81323. V002T02A008.

[43] Skamarock William C, Klemp Joseph B. A time-split nonhydrostatic atmospheric model for weather research and forecasting applications. J Comput Phys 2008;227 (Issue 7):3465–85. https://doi.org/10.1016/j.jcp.2007.01.037. ISSN 0021-9991.

[44] Saha S, Moorthi S, Pan H, Wu X, Wang J, Nadiga S, Tripp P, Kistler R, Woollen J, Behringer D, Liu H, Stokes D, Grumbine R, Gayno G, Wang J, Hou Y, Chuang H, Juang HH, Sela J, Iredell M, Treadon R, Kleist D, Van Delst P, Keyser D, Derber J, Ek M, Meng J, Wei H, Yang R, Lord S, van den Dool H, Kumar A, Wang W, Long C, Chelliah M, Xue Y, Huang B, Schemm J, Ebisuzaki W, Lin R, Xie P, Chen M, Zhou S, Higgins W, Zou C, Liu Q, Chen Y, Han Y, Cucurull L, Reynolds RW, Rutledge G, Goldberg M. The NCEP climate forecast system reanalysis. Bull Am Meteorol Soc 2010;91(8):1015–58. Retrieved Nov 25, 2022, from, https://journals.ametsoc.org/view/journals/bams/91/8/2010bams30.

[45] Komen G, Cavaleri L, Donelan M, Hasselmann K, Hasselmann S, Janssen P. Dynamics and modelling of ocean waves. Cambridge: Cambridge University Press; 1994. https://doi.org/10.1017/CBO9780511628955.

[46] Tolman HL. User manual and system documentation of WAVEWATCH III TM version 3.14. 2009 [Technical report].

[47] Mentaschi L, Besio G, Cassola F, Mazzino A. Developing and validating a forecast/hindcast system for the Mediterranean Sea. Journal of Coastal Research, SI 2013;65:1551–6. JCR 65.

[48] Mentaschi L, Besio G, Cassola F, Mazzino A. Performance evaluation of WavewatchIII in the Mediterranean Sea. Ocean Model 2015;90:82–94. https://doi.org/10.1016/j.ocemod.2015.04.003OM90.

[49] Standard: IEC 61400-1 wind turbines part 1: requirements. International electrotechnical commission; 2015.

[50] Rice SO. Mathematical analysis of random noise. Bell Syst. Tec. J. 1945;23:282–332.